



# Haze Seasonal Variations of Titan's Upper Atmosphere during the Cassini Mission

Benoît Seignovert<sup>1,2</sup> , Pascal Rannou<sup>2</sup> , Robert A. West<sup>1</sup> , and Sandrine Vinatier<sup>3</sup>

<sup>1</sup> Jet Propulsion Laboratory, California Institute of Technology, Pasadena, CA 91109, USA; [research@seignovert.fr](mailto:research@seignovert.fr)

<sup>2</sup> GSMA, Université de Reims Champagne-Ardenne, UMR 7331-GSMA, 51687 Reims, France

<sup>3</sup> LESIA, Observatoire de Paris, Université PSL, CNRS, Sorbonne Université, Université de Paris, 5 place Jules Janssen, 92195 Meudon, France

Received 2020 January 30; revised 2020 October 6; accepted 2020 October 21; published 2021 January 25

## Abstract

This study presents a 13 yr survey of haze UV extinction profiles, monitoring the temporal evolution of the detached haze layer (DHL) in Titan's upper atmosphere (350–600 km). As reported by West et al. (GRL vol.38, L06204) at the equator, we show that the DHL was present at all latitudes below 55°N during the northern winter (2004–2009). Subsequently, it globally sunk and disappeared in 2012. No permanent DHL was observed between 2012 and 2015. Only in late 2015 did a new structure emerge from the Northern hemisphere, and propagate to the equator. This new DHL is not as pronounced as that observed in 2004, and is much more complex. In one specific sequence, in 2005, we were able to investigate the short timescale variability of the DHL, and no major changes were observed. When both sides of the limb were visible (dawn/dusk), we notice that the extinction of the DHL is slightly higher on the dawn side. Moreover, during a polar flyby in 2009, we observed the longitudinal variability of the DHL and spotted some local inhomogeneities. Finally, comparisons with UVIS stellar occultations and General Climate Models are both consistent with our findings. However, we noticed that the timing of the DHL main pattern predicted by the GMCs can be off by up to 30° in solar longitude. All these observations offer new perspectives on the seasonal cycle of Titan's upper atmosphere, the evolution of the DHL and its interaction with the dynamics.

*Unified Astronomy Thesaurus concepts:* [Saturnian satellites \(1427\)](#); [Radiative transfer \(1335\)](#)

## 1. Introduction

Titan is the only moon of the solar system with a thick hazy atmosphere, which represents approximately 20% of its apparent diameter. This atmosphere is mainly composed of nitrogen and methane. The photodissociation of these molecules by the UV light in the upper part of the atmosphere leads to the production of a large number of other hydrocarbons and nitriles as trace species, and to photochemical haze. This haze is global and completely covers Titan. It controls the thermal balance via its visible and thermal infrared properties (e.g., Bézard et al. 2018). It also veils the lower atmosphere, and the surface that can be perceived in a few methane windows, in near-infrared.

Titan's haze was first resolved in the 80s by Pioneer 11 (Smith 1980) and the two Voyagers (Smith et al. 1981, 1982; Sromovsky et al. 1981). It had several remarkable structures: a northern (winter) polar hood, an interhemispheric asymmetry, and a thin global detached haze layer (DHL) above the main global haze layer. It was thought that the detached haze layer had a dynamical origin (Smith et al. 1981). Photometric analyses provided a means to derive the extinction properties of both haze layers and to evaluate the effective radius of the aerosols in the detached haze ( $\simeq 0.3 \mu\text{m}$ ) and in the main haze ( $\simeq 0.4 \mu\text{m}$ ) layers (Rages & Pollack 1983; Rages et al. 1983). Analysis of Voyager images showed that the detached haze layer appears due to a strong depletion of aerosol extinction around 300 km, yielding a distinct layer above the main haze layer, with a maximum extinction located around 350 km (Rages & Pollack 1983). Its horizontal extent was very stable in pressure, and it was reported at all southern latitudes up to 45°N, where it connected to the northern polar hood. The detached haze layer was re-observed twenty years after the Voyager flybys, during Cassini's first flyby in 2004 (Porco et al. 2005). The main change was in its altitude location at 500 km, which was 150 km higher than in

1981. Again, it appeared as a fairly homogeneous global shell above the main haze layer at a constant altitude, and merged with the northern polar hood. Notably, while Voyager observations were performed after the northern spring equinox, Cassini's early observations occurred during the northern winter, i.e., half a season earlier (Figure 1).

Toon et al. (1992) first attempted to explain the observation of the DHL. They used a 1D microphysical model, whereby an ad hoc vertical wind maintains the DHL particles at a constant altitude above the main haze layer. Alternative scenarios have been proposed to explain the DHL from purely microphysical processes. Chassefière & Cabane (1995) investigated the case for two different aerosol production layers. They proposed that the uppermost layer (500–1000 km) produces fluffy aggregates that could be swept horizontally by winds, generating a detached haze layer. They also proposed an alternative scenario where aerosols settle downward and interact with macromolecules from the main haze layer, produced by the lower production zone (around 350–400 km). In the latter case, the interaction would produce a significant optical gap. However, they favored the scenario involving winds which would match all the constraints known at that time. In the same vein, Lavvas et al. (2009) proposed a scenario based on a purely microphysical process. Aerosols are produced at high altitude, as per the Chassefière & Cabane (1995) hypothesis, growing as spheres down to levels around 500 km. There, the detached haze is produced by a sudden change in the fractal dimension of the aerosols. This produces a sharp change in microphysical properties, and an artificial optical gap. However, it is unclear how this model for the production of the detached haze layer would be augmented to account for the seasonal evolution with respect to altitude, disappearance, and reappearance (as described below).

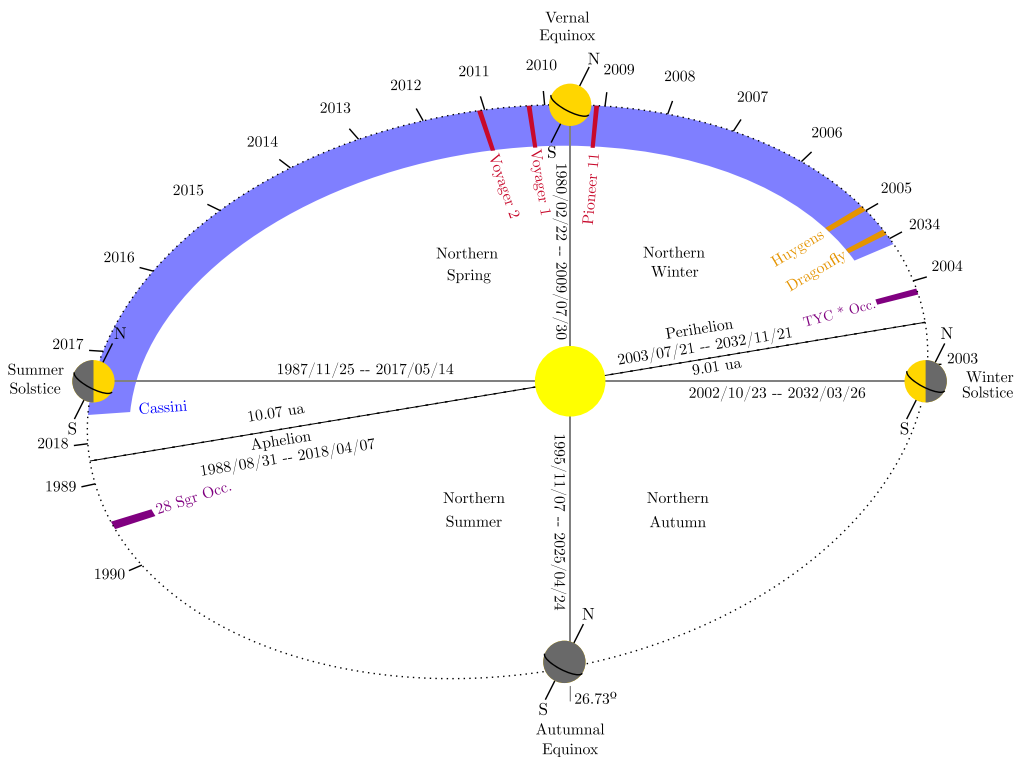


**Figure 1.** Titan's orbital position as a function of the season, reported as solar longitude position ( $L_s$ ). The Cassini mission covered almost half a Titan year. The Pioneer and Voyager flybys are also reported, as well as the Huygens landing, and ground-based stellar occultations observed on Earth.

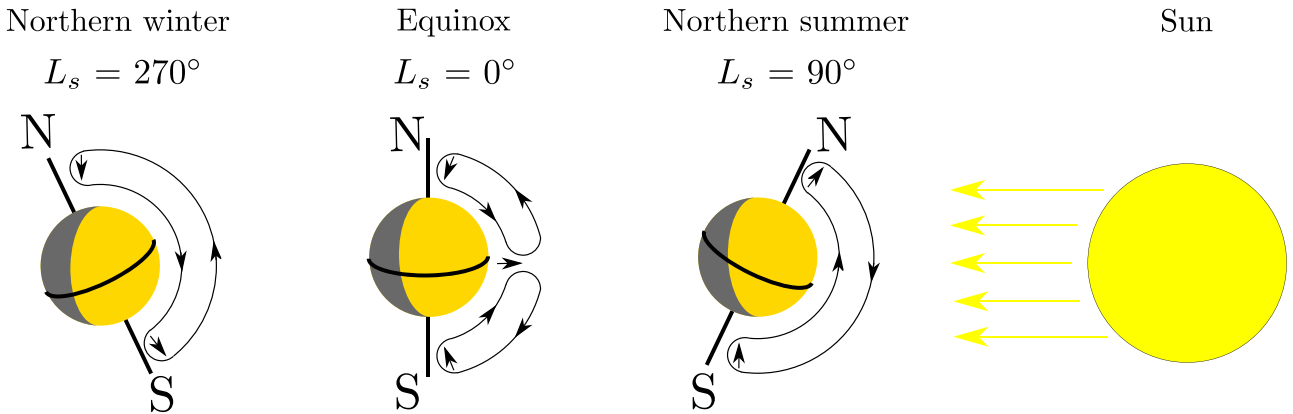


**Figure 2.** Synthetic representation of Titan atmospheric circulation as a function of season.

Later, with a 2D-General Climate Model (GCM) accounting for the transport of haze by dynamics and the radiative feedback, it became possible to reproduce and explain the mechanism that produces the DHL (Rannou et al. 2002). It was also demonstrated that this feedback strongly enhances the wind speed, due to the thick polar haze cap near the winter pole. In return, this cap enhances the cooling to space during the polar night (Rannou et al. 2004) and reinforces the circulation. Due to Titan's obliquity ( $27^\circ$ ) and slow rotation rate, seasons are well marked, and Hadley circulation cells span both hemispheres. This situation leads to the formation of a broad ascending circulation in the summer hemisphere, capable of lifting aerosols to high altitudes, where they remain suspended and are transported through mid-latitudes to the winter polar region, where they are transported by subsidence (Figure 2). In this scenario, the location of the DHL corresponds to the area where the settling speed is compensated by upward winds, and evolves

with seasonal changes of illumination. More sophisticated 3D-GCMs led to an improved understanding of the haze cycle, including the formation of the detached haze, and confirmed this picture (Lebonnois et al. 2012; Larson et al. 2015). This formation mechanism implies that the DHL is a blending of aerosols newly produced and falling from above, and older and larger aerosols, produced in the stratosphere and lifted by circulation. Although the GCM results differ in some aspects with observations, they are able to capture the big picture behind the existence of the DHL.

Photometric studies performed with Cassini data taken before the equinox in 2009 provide complementary observations of the DHL (Cours et al. 2011; Koskinen et al. 2011; Seignovert et al. 2017). On one hand, the authors used the light intensity scattered at the limb in UV (338 nm) at different phase angles, measured by the ISS. On the other hand, a single value of the tangential opacity in VUV (187 nm) was retrieved from

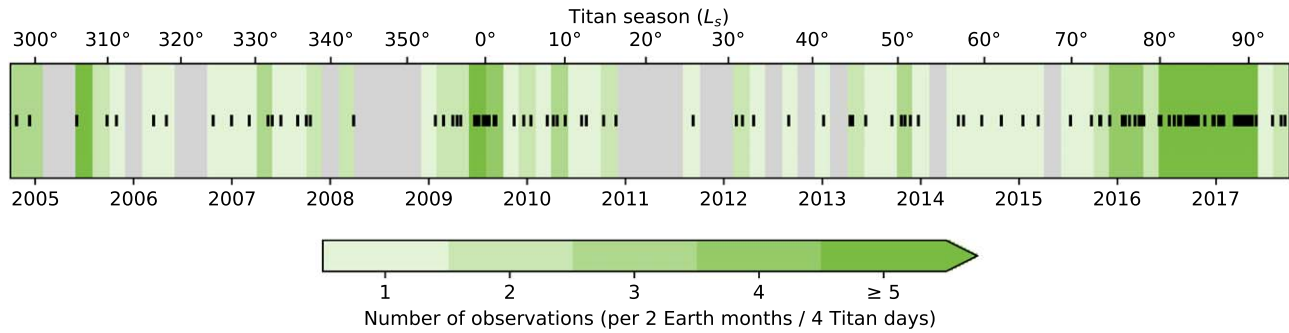


**Figure 3.** Timeline of the ISS/NAC CL1-UV3 images analyzed (vertical black ticks). The number of observations per period of 2 Earth months (i.e., 4 Titan days/ $\Delta L_s \approx 2^\circ$ ) is represented by a green gradient scale. The gray areas correspond to gaps with no available observations.

UVIS observations during stellar occultations. The results show the presence of large aerosols in the DHL, with an effective bulk radius  $\approx 0.2 \mu\text{m}$ , producing all the UV scattering, while small nanometric aerosols are needed to explain most of the VUV extinction (Cours et al. 2011), which is quite consistent with a DHL composed of two different populations of aerosols.

West et al. (2011) also reported a rapid collapse of the detached haze layer, starting just before the equinox. The altitude of the DHL descended by about 80 km in 200 terrestrial days, and by 30 km more in about 300 terrestrial days. A simple extrapolation of the altitude of the DHL with time indicated that it would be at the same altitude as observed by Voyager exactly one Titan year after the Voyager epoch. West et al. (2011) concluded that such a result was coherent with a seasonal cycle of the DHL. They compared their results with a 2D-GCM (Rannou et al. 2002) and made a prediction about the reappearance of the DHL several years later (2013–2016) at its initial altitude (around 500 km). Lebonnois et al. (2012) and Larson et al. (2015) made similar predictions, but with a reappearance of the DHL a bit later, around the next northern summer solstice ( $L_s = 95^\circ$  and  $70^\circ$ – $80^\circ$ , respectively). In practice, West et al. (2018) found that the DHL reappeared in early 2016 ( $L_s = 73^\circ$ – $76^\circ$ ) at 480 km, several months before the solstice (mid-2017). They followed the cycle of the DHL at the equator and retrieved the haze extinction profile in the CL1-UV3 filter combination. Its reappearance was much more complex than predicted. This early 2016 detached haze layer dropped in altitude down to 470 km within a terrestrial year and vanished, while a new DHL emerged again around 500 km. This new layer appeared quite stable until the end of the Cassini mission (2017 September,  $L_s = 91^\circ$ ). Unfortunately, no other data exist to further probe the DHL, and nothing is known about the fate of the detached haze after this date.

In this work, we perform a systematic latitude–altitude mapping of the detached haze layer in the range of 350–600 km altitude. This covers the period between 2004 July (half a season after the northern winter solstice) and the end of the mission in 2017 September (after the summer solstice). We used all the UV3 observations acquired by the Cassini Narrow Angle Camera (NAC) of the ISS. We used exactly the same model as West et al. (2018), i.e., a ray tracing model in spherical shell geometry for the single scattering albedo, and a correction for multiples scattering.

The outline of the article is as follows: in the next section (Section 2), we first give a global presentation of the available data and the criteria we use to select images. Then we describe the main principle of the retrieval model and the retrieval method. In Section 3 we present the results of the photometric analysis as latitude–altitude panels, showing the spatial distribution of the

DHL and the upper part of the main haze layer. The seasonal cycle of the DHL is split into four specific periods between 2004 and 2017. This section has 4 subsections, one for each period, where we explain in detail the main characteristics of the haze and its evolution. Section 4 is dedicated to the study of specific sets of observations that probe short timescales, short-term, or diurnal variations. We first describe how the data were selected and then what they reveal about Titan’s atmosphere. In Section 5, we make comparisons between our results and those obtained at the same location and the same time from UVIS. We also make comparisons between our results and the prediction made by two Titan 3D-GCMs with regard to the detached haze layer and its evolution. The conclusion and the perspective of this work are given in Section 6.

## 2. Observations and Models

### 2.1. Selection of Observations

We conduct our survey based on 138 images<sup>4</sup> taken by the Cassini Image Science Sub-System Narrow Angle Camera (ISS–NAC) with the clear and ultraviolet filter combination CL1-UV3. At this wavelength (338 nm), ISS is sensitive to haze in the upper part of Titan’s atmosphere (300–600 km altitude). We choose the best samples from the 317 images available on the NASA Planetary Data System (PDS) to obtain the highest temporal and phase coverage. For the main study we kept only images taken with at least a one day gap. We also kept specific sets of observations made a few hours apart in order to study short-term variations.

On average, the selected images are separated by 39 Earth days, i.e., 2.5 Titan days (Figure 3). Although our sampling is not evenly distributed, due to orbital constraints and mission schedule, at least 90% of the selected images are separated by less than 120 Earth days, i.e., 7.5 Titan days. Two main gaps in the data can be observed. The first is between 2008 March 28 and 2009 January 25 (302 Earth days/19 Titan days), and the second between 2010 November 26 and 2011 September 9 (286 Earth days/18 Titan days).

The selected images are calibrated using the CISSCAL routines (v3.8) provided on the Planetary Data System. To improve the signal to noise ratio on the limb profile, we deconvolved the images with a Poisson Maximum A Posteriori method, using the point-spread function measured in-flight (West et al. 2010; Knowles et al. 2020). This deconvolution method is known to be efficient in restoring fine structures in astronomical images

<sup>4</sup> See Data Availability section for the list and the results for all analyzed ISS images.

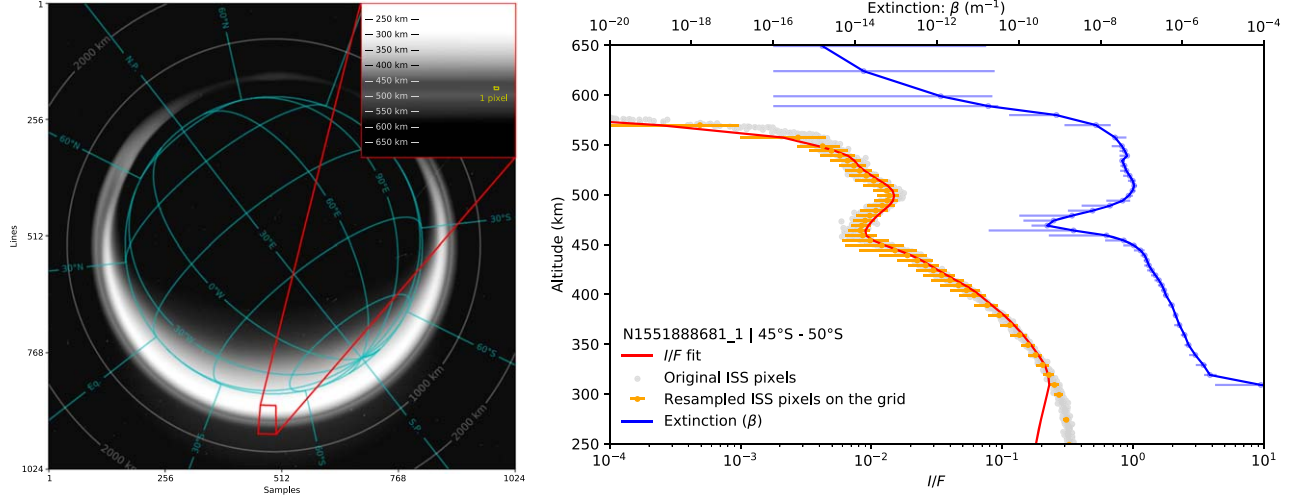


**Figure 4.** Left: Log scale representation of the  $I/F$  for the image N1551888681\_1, taken in 2007 March. The data are sampled at the limb by bins of  $5^\circ$ . The red area corresponds to the bin at the photometric equator ( $[45^\circ\text{S}, 50^\circ\text{S}]$  and  $[76^\circ\text{W}, 79^\circ\text{W}]$ ). The pixel scale (7.9 km) is represented in the zoomed area by the yellow rectangle. An altitude grid is also depicted, where we can see the peak of intensity of the DHL located at 500 km. Right: the red curve represents the inverted  $I/F$  profile fitted on the resampled data (orange error bars) within a  $5^\circ$  bin in latitude. The uncertainties on the retrieved extinction profile  $\beta$  (in blue) are calculated to match the  $1\sigma$  distribution of the  $I/F$  pixels. The model fits the observations down to 300 km. The uncertainties increase rapidly when the observed ( $I/F$ ) is close to the noise level ( $3 \times 10^{-3}$ ).

(Hunt et al. 1996). In our case, the main source of light is always Titan, and is resolved inside the field of view of the camera (Figure 4(a)). Therefore, we do not expect to see a significant contribution from stray light in this configuration (West et al. 2010). The image pointing is initialized with SPICE kernels (Acton 1996; Annex et al. 2020). Since the surface of Titan is not visible in the UV, we improved the location of Titan’s center by fitting the limb intensity. We then calculated the planetocentric coordinates of each pixel, and their tangent point altitude with respect to a mean spherical body with a radius of 2575 km.

Intensity profiles are extracted every  $5^\circ$  on both sides of the limb. Depending on the latitude of the Sub-Cassini point on the ground, the sampling in latitude is not evenly distributed for each image. Therefore, the polar latitudes are usually less covered than the equator. In addition, the solar illumination changes drastically during the season between the northern midwinter to summer, which restricts our ability to see both poles at the same time. On average, the image pixel scale is about  $10 \pm 5$  km.

## 2.2. Model of Scattering at the Limb

To retrieve the haze extinction profiles from the intensity observations, we model the synthetic radiance factor ( $I/F$ ) with a single scattering ray tracing model in a spherical shell geometry. The effect of multiple scattering is accounted for as a correction,  $\varrho_k(z)$ , applied to the volume scattering along line of sight. This technique has been used successfully several times (e.g., Rages & Pollack 1983; Rannou et al. 1997; Seignovert et al. 2017; West et al. 2018).

In the detached haze layer, the multiple scattering is mainly produced by the light coming from the main haze below. To evaluate  $\varrho_k$ , we use a representative vertical profile of the main haze that reproduces the observed intensity of Titan in the UV. With a radiative transfer model (SHDOMPP, from Evans 1998) we have access to the complete radiative source function at each level of the atmosphere, as well as the optical properties (haze absorption and scattering and Rayleigh scattering). We are then able to compare the intensity scattered in the direction

of the observer from the direct Sun only, and from the direct Sun and the scattered field coming from below.  $\varrho_k$  is defined as the ratio of multiple scattering to single scattering toward the observer for a given altitude, and as a function of the incident and emergent angles. This parameter is pre-computed as a function of altitude, incident, and emergent angles, and saved in a look-up table (see West et al. 2018, for details). We find that the multiple scattering increases the scattered intensity at the limb of Titan in the UV by a ratio between 1.05 and 1.20, depending on the geometry of the observation. This effect is included in our model. We also verified that significant changes in the main haze (single scattering albedo, opacity, and vertical scale height) only affect the value of  $\varrho_k$  by a few percent and can be neglected.

We discretize the atmosphere in  $N = 60$  irregular layers of various thickness:  $\Delta z = 50$  km from the ground to 200 km,  $\Delta z = 25$  km from 200 to 300 km,  $\Delta z = 10$  km from 300 to 400 km and from 550 to 700 km. Finally, we used  $\Delta z = 5$  km between 400 and 550 km. This grid allows us to take advantage of the spatial resolution of the ISS–NAC camera in the region of interest, where the DHL is primarily located.

We can write the outgoing  $I/F(z)$  as:

$$I/F(z) = \sum_{i=0}^{n_x-1} \int_{x_k}^{x_{k+1}} \frac{\langle \varpi P(\Theta) \rangle_k}{4} e^{-(\tau_k^i(z) + \tau_k^e(z))} \times \beta_k(z) \varrho_k(z) dx \quad (1)$$

where the summation is performed on the  $n_x - 1$  segments defined by the intersections of the line of sight and the spherical shell boundaries. The impact parameter  $z$  (the lowest altitude reached by the line of sight) is given by the bottom of the  $n$ th layer crossed.  $x$  is the abscissa along the line of sight.  $\tau_k^i$  and  $\tau_k^e$  are the opacities along the incident and emergent paths.  $\langle \varpi P(\Theta) \rangle_k$  is the average of the product of the single scattering and the phase function at the scattering angle of the observation  $\Theta$  for the layer crossed on  $x_k$ .  $\beta_k(z)$  is the local extinction coefficient at altitude  $z$  (and the product of the haze cross-

section and the local number density). Here, the altitude  $z(x)$  is the local altitude at the point of abscissa  $x$  along the line of sight.

### 2.3. Retrieval Method

Based on our previous work (Seignovert et al. 2017; West et al. 2018), we make the assumption that the optical properties,  $\langle \varpi P(\Theta) \rangle_k$ , of the aerosols are constant in the upper part of Titan's atmosphere. This allows us to focus our study only on the retrieval of the extinction along the line of sight. In our model, the  $I/F(z)$  intensity profiles depend on the set haze extinction profile  $\beta(z)$  and the viewing geometry of the observation (incidence, emergence, and phase angles). We assume no horizontal inhomogeneity along the line of sight (Seignovert et al. 2017). We retrieve a set of extinction values,  $\beta_i$  (the vector  $\beta$ ), with  $i$  denoting the indices of the layers, that matches the values of the  $I/F_i$  (the vector  $I/F$ ).

From Equation (1), it is possible to cast the scattered intensity,  $I/F_i$ , as a function of the extinction  $\beta_j$  with  $j \leq i$ . This forms a nonlinear triangular system. To find the vector  $\beta$ , we have to solve the formal equation:

$$I/F = G(\beta) \quad (2)$$

where  $G$  is a nonlinear function which depends on  $\beta_i$  and on the viewing geometry of the observation.

We solve the system by globally minimizing the difference between the modeled  $I/F$  and the observations, using a Levenberg–Marquardt minimization. Therefore, we simultaneously obtain all the  $\beta_i$  at once. Moreover, the tangential opacity along a line of sight ( $\tau_{\text{los}}$ ) is considered opaque when it reaches 3 (usually around 300 km in the UV). Beyond this threshold, we do not retrieve the value of  $\beta$ . An example of inversion is presented in Figure 4.

The uncertainties associated to the intensity profile ( $I/F$ ) correspond to a  $1\sigma$  distribution of the observed  $I/F$  for a given altitude within a  $5^\circ$  bin in latitude. The number of pixels within a  $5^\circ$  bin varies from one image to another, and depends on the viewing geometry and the altitude sampled. Usually we have more than 1500 pixels per profile between 0 and 700 km. In the worse case scenarios (N1630432142\_1 at  $6\sigma$  of the average pixel scale) we have at least 120 pixels per profile. This allows us to resample our observed profile on a vertical grid with layers smaller than the image pixel scale in the 500 km region. The uncertainties in the extinction profile ( $\beta$ ) correspond to the minimum and maximum values required to fit the data within  $1\sigma$  of the observed  $I/F$  in each layer independently (contrary to West et al. 2018, where the errors were computed in all the layers simultaneously).

## 3. Seasonal Cycle of the Haze Extinction

In order to provide a detailed explanation of the complex latitudinal variability of the detached haze layer, we present some of the key images that we have analyzed. Based on our previous work, focused on the evolution of the detached haze in the equatorial region (West et al. 2018), we define four different seasonal phase characteristics of the evolution of the detached haze layer. Between 2004 and 2008, the DHL was stable in altitude and extinction profile. Between 2008 and 2012, it settled and disappeared in the main haze below the 300 km. During the period 2012–2016, the DHL was not observed, and only sporadic transitory layers showed up in the

UV3 images. After 2016, and up to the end of the Cassini mission, the DHL reappeared, following a complex pattern. Here we illustrate the complete time and latitude survey, covering a period of time which includes about half a Titan year. This is valuable because it encompasses the equinoctial transition period of 2009. For each phase, we display the altitude and latitude distribution of the instantaneous haze extinction coefficient retrieved from intensities at the illuminated limb of Titan. The same color scale is applied to all the panels in order to maintain a consistent view for the whole data set. It corresponds to the range where the model exhibits the best sensitivity at UV wavelengths. In some cases, smaller features might be harder to highlight with this color scheme; however, all the results from these panels are available to the reader for more in depth considerations (see Data Availability section). Locations where no data are available are left as blank areas on the panels.

### 3.1. Period 1: A Very Well Delimited Detached Haze Layer During the Northern Winter (2004–2008)— $L_s = 300^\circ$ – $340^\circ$

On its arrival in the Saturnian system in 2004, Cassini observed a single detached haze layer at 500 km altitude (Figure 5(a)) similar to that observed at 350 km by Voyager 24 years earlier (Smith et al. 1981). At that moment, Titan was two years past its winter solstice in the northern hemisphere, at  $L_s = 300^\circ$ . With Cassini, we see that in the southern hemisphere, the haze layer was completely detached from the main haze layer. The haze extinction was at least one order of magnitude smaller inside the depleted zone (470 km) than in the main and the detached haze layers (below 450 and at 500 km, respectively). Between the equator and up to about  $60^\circ\text{N}$  it exhibited a local depletion in extinction of a factor 10. There, the separation with the main haze is not as distinct as in the south, but is still sufficiently significant to define a detached haze layer. The altitude of the depletion zone decreased by about 50 km between the latitudes  $30^\circ\text{N}$  and  $60^\circ\text{N}$ . The detached haze layer merged with the polar hood beyond  $60^\circ\text{N}$ . This description of the detached haze layer at the beginning of the Cassini mission is very consistent with the results obtained from stellar occultation in 2003 (Sicardy et al. 2006). Throughout the period 2004–2008, the detached haze layer was quite stable in shape and altitude, with a maximum of extinction at  $500 \pm 20$  km. The top of the main haze layer was located around  $450 \pm 20$  km below  $30^\circ\text{N}$ , and dropped by 50 km between  $30^\circ$  and  $60^\circ\text{N}$ .

However, there are noticeable variations in haze extinction. The detached haze remained stable over several months, but in 2004 December (Figure 5(b)), the detached haze layer extinction was found to be a factor of 10 lower than previously observed at almost all latitudes south of  $30^\circ\text{N}$ , and about half a decade above  $30^\circ\text{N}$ . The polar hood and the main haze do not show a similar decrease. In the following periods, (Figures 5(c), (d) and (e)), the detached haze was partially restored, but not with the same amount of extinction as before. Only observations in 2007 (Figure 5(f)) show extinctions in the detached haze layer comparable to those seen before the decrease. We note that the decrease of extinction below 370 km in the polar hood above  $50^\circ\text{N}$  (Figure 5(e)) is at the limit of sensitivity of the UV filter. The stability of the large-scale structure of the detached haze layer is related to the steady state of the large-scale circulation throughout the winter. The observation of 2007 October (Figure 5(f)) is the last view that we have of this stable state before the seasonal turnover.

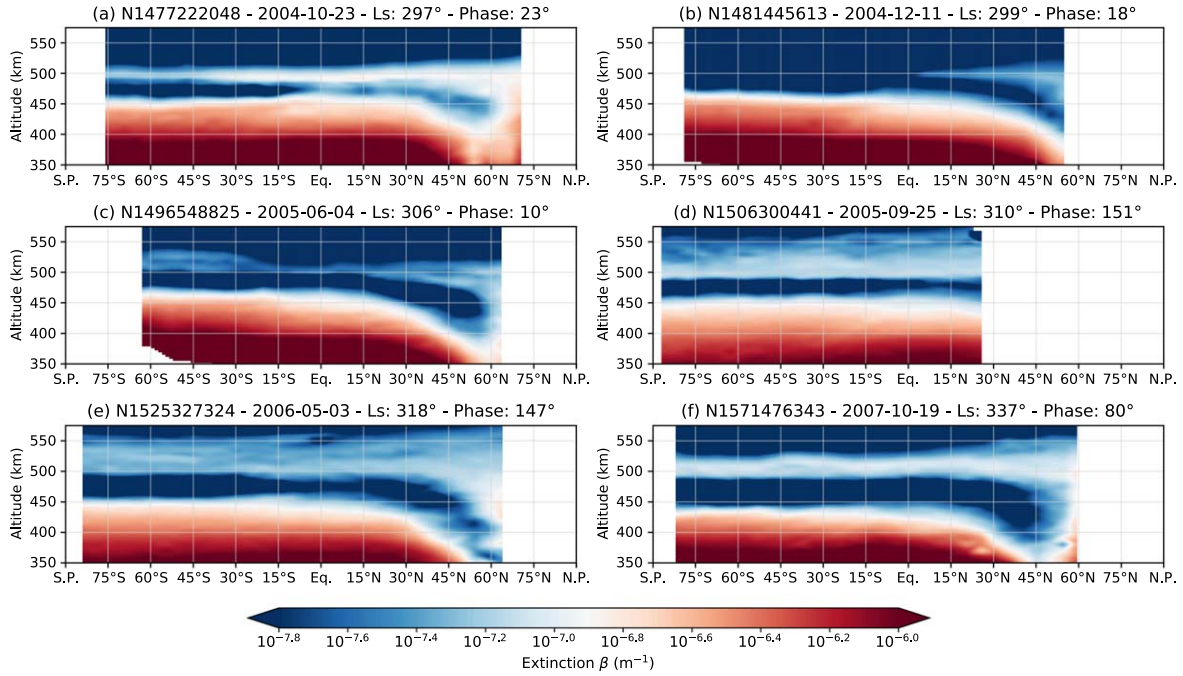


**Figure 5.** Latitudinal haze extinction profile ( $\beta$ ) retrieved for 6 images taken between 2004 and 2008 ( $L_s = 300^\circ\text{--}340^\circ$ ), showing a stable DHL at  $500 \pm 20$  km altitude. The color schema is fixed for all the figures, to enable direct comparison between the different panels. The seasonal solar longitude ( $L_s$ ) and the observation phase angle are also provided in each panel.

During this period, the detached haze also has a strong layering with, at some latitudes, distinct decks which are not continuous, and rather appear as foliation. This feature is more pronounced in some observations, for instance from 2005 June to 2006 May, but does not show up in 2007 October, except marginally beyond  $30^\circ\text{N}$ . The foliated detached haze layer has a larger geometrical thickness than before 2004 December.

As we will see in Section 4, the detached haze layer exhibits some longitudinal or diurnal variability, which limits our ability to interpret details of features observed in single images. The small-scale features could depend on local short-term dynamics, such as inertia-gravity waves.

### 3.2. Period 2: Drop and Disappearance of the Main Haze Layer Around the Vernal Equinox (2008–2012)— $L_s = 340^\circ\text{--}30^\circ$

A precursor sign of the drop in the detached haze can be seen in 2008 March (Figure 6(a)). The main haze starts an initial contraction around  $35^\circ\text{S}$ . There, the depleted zone is almost 75 km thick at its maximum. In 2009 January, the main haze continued to fall from 425 km down to 375 km, while the detached haze layer remained around 500 km (Figure 6(b)). Following the drop in the main haze in early 2009, the detached haze starts its own descent in 2009 June, just before the equinox (Figure 6(c)). This delay in collapse increased the apparent thickness of the depletion zone between the two haze layers.

As for the main haze, the detached haze collapses first in the Southern hemisphere, from 500 to 425 km, and then at the equator and in the northern hemisphere (Figure 6(c)). This is associated with the circulation turnover affecting the summer hemisphere ascending branch first. Over time, the detached haze gradually settled in altitude, and finally disappeared below 300 km. Later ISS observations made using blue and green filters show that the main DHL continues its descent below

300 km during 2011. Since our current model was only tested for UV observations, we were not able to observe its merger with the main haze. The complete collapse of the detached haze, as it appeared in the UV3 filter, is displayed in Figures 6(c)–(h). We note that the column extinction is smaller at the equator than at other latitudes, and that this is the case during the entire period of the collapse.

During the fall, a second thin detached haze layer, at planetary scale, is evident above the collapsing detached haze layer. In 2010 January (Figure 6(e)), the detached haze layer was located between 375 and 400 km. We can still see a double deck of haze, and this time the detached haze appears higher at the equator compared to the two hemispheres, producing an arch. The haze peak extinction has globally increased by a factor of two, due to sedimentation in denser layers.

In 2010 August (Figure 6(f)), one year after equinox, the detached haze layer continued its drop down to 375 km at around  $40^\circ\text{S}$ , and 400 km at the equator. It had gained in complexity, with multiple secondary layers up to 520 km. The detached haze formed a remarkable arch with a difference of about 50 km in altitude between the equator and the poles, as previously noticed by West et al. (2011). This observation and the next correspond to the same seasonal phase of Voyager flybys ( $L_s = 8^\circ$  and  $18^\circ$ ). They can be compared directly. We now know that this season was a time of rapid change, and that the Voyager probes observed transient situations. Voyager also observed the detached haze to be higher near the equator than elsewhere (Rages & Pollack 1983; Rannou et al. 2000).

Due to orbital constraints and mission planning, the next observation was made in 2011 September (Figure 6(g)). The detached haze layer was, at that time, well below the level of the polar hoods. Again, secondary detached layers show up as high as 470 and 520 km.

The south polar hood was not present in 2010 August (Figure 6(f)), and appeared in less than 13 months. This

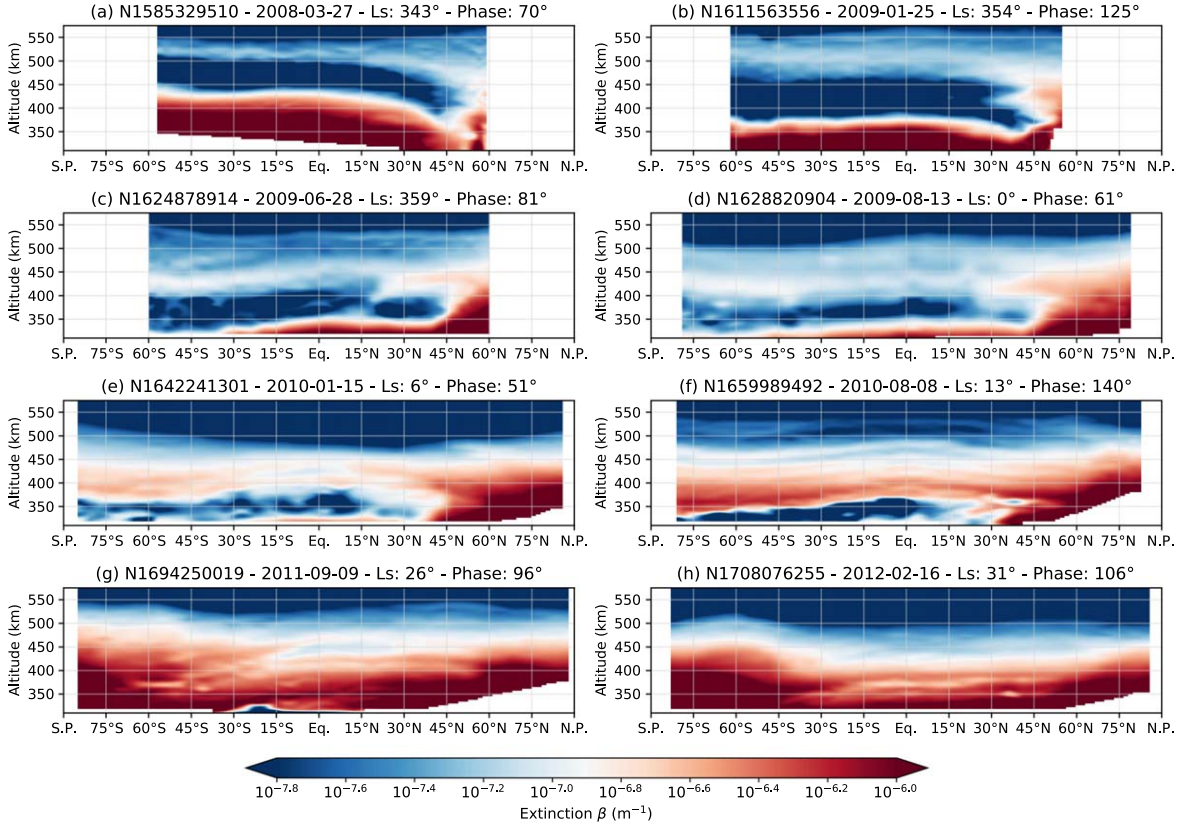


**Figure 6.** As Figure 5, but for 8 images taken between 2008 and 2012 ( $L_s = 340^\circ\text{--}30^\circ$ ), showing the drop and disappearance of the DHL. The color schema is identical to that in Figure 5 so as to provide direct comparisons. In this case, the altitude range is extended down to 300 km (where the model becomes less reliable).

indicates that the circulation started to reverse around the equinox, and that the southward circulation sent haze to the southern polar region and produced a polar hood. The change in haze distribution is a very good indication of the timing of the equinoctial circulation turnover, as discussed below. We note that the strong haze depletion at 300 km and between  $30^\circ\text{S}$  and  $20^\circ\text{N}$  is real (and visible in the  $I/F$  profiles), but may be exaggerated at  $20^\circ\text{N}$  due to the limitations of the retrieval procedure. At this altitude level, Titan's atmosphere is opaque to UV radiation (see Figure 4), and does not allow us to follow the main depletion below this altitude.

The last UV3 image we have showing a detached haze layer was taken in 2012 February (Figure 6(h)). At that time, the initial detached haze had completely disappeared, and the secondary detached haze layer was still descending and had reached 400 km altitude. The secondary detached haze layer is not well delineated by a layer strongly depleted in aerosols. The south polar hood had increased its latitudinal extent northward to  $50^\circ\text{S}$  and become larger than the northern polar hood, which tended to retreat.

### 3.3. Period 3: Absence of the DHL, with Sporadic Transitory Layers After the Northern Spring Equinox (2012–2015)— $L_s = 30^\circ\text{--}75^\circ$

During this period (Figure 7), the main haze layer has large-scale structures which slowly evolve under the influence of large-scale circulation. The south and north polar hoods are still visible, and evolve with time. Superimposed on this background haze, transient structures show up and disappear from

one observation to the other. At some moments, large-scale detached hazes appear. They differ from the detached haze seen at the beginning of the mission because they are not stable in time and in altitude.

In 2012 April (Figure 7(a)), the detached haze has completely disappeared, except for some residual structures at 370 km around the equator. These relics of the last detached haze layer are almost imperceptible in the corresponding  $I/F$  profile. At other latitudes, we can see only the main haze with a marked south polar hood, and a small increase of extinction above  $65^\circ\text{N}$  which could be the residual north polar hood. Sometimes, detached layers emerge from the background with large latitudinal extent (e.g., the detached haze at 500 km in Figure 7(b)). However, these only remain for a short time, and are not seen in the following observations.

In 2014 August (Figure 7(c)) we observed a plume of aerosol between  $10^\circ\text{S}$  and  $25^\circ\text{N}$ , reaching 530 km. A detached haze layer seems to spread from this plume toward the north and the south. This detached haze is around 500 km in altitude, descending to 470 km at  $50^\circ\text{S}$  (and probably even further south). In the north, the detached haze does not extend further than  $50^\circ\text{N}$  and remains at 500 km. This indicates an atmosphere circulation flowing from the equator toward the south pole. These aerosols seem to originate from the equatorial part of the main haze.

Most of the observations between 2012 and the end of 2015 are featureless, as shown in Figure 7(d) taken in 2015 October. During this period, the main haze has a uniform scale height of 45 km, with an homogeneous extinction at the planetary scale.

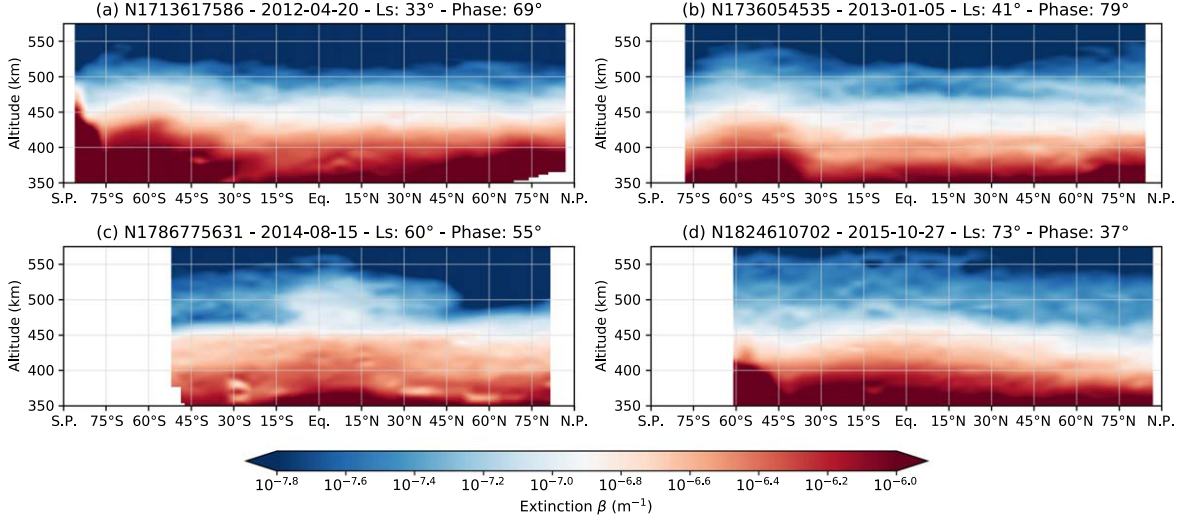


**Figure 7.** As Figures 5 and 6, but for 4 images taken between 2012 and 2015 ( $L_s = 30^\circ\text{--}75^\circ$ ), showing sporadic transitory layers and the absence of a stable DHL. The color scheme is the same as in previous figures, and the altitude extends down to 350 km.

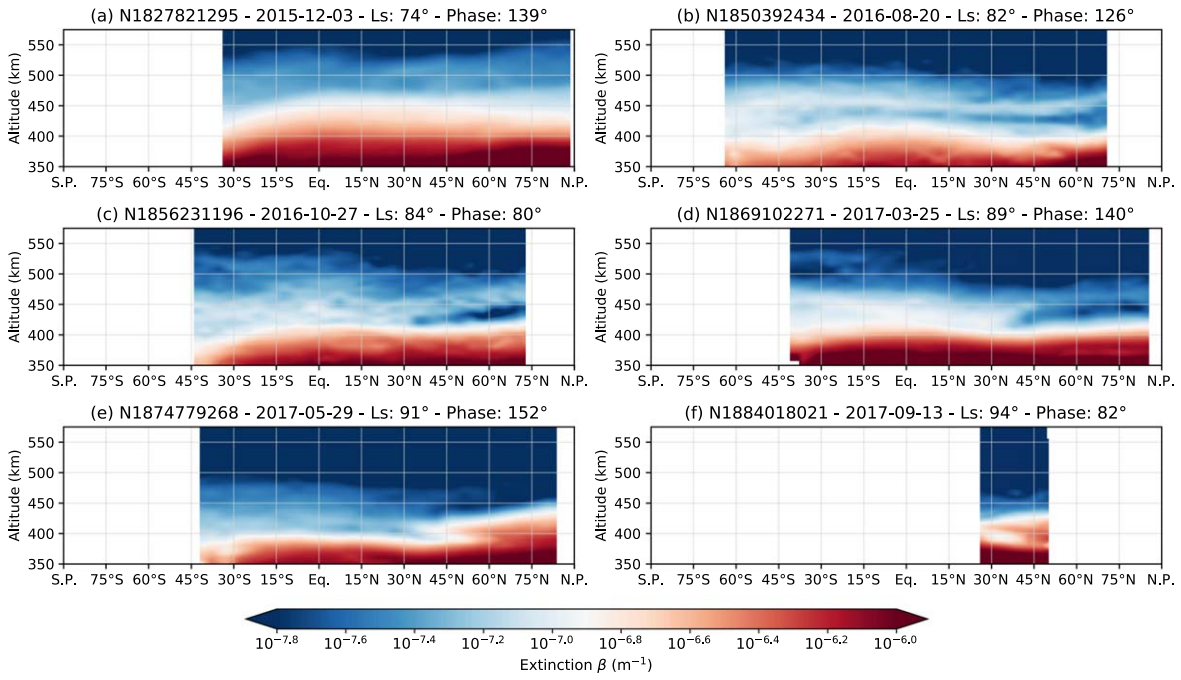


**Figure 8.** As the Figures 5–7, but for 6 images taken between 2015 and 2017 ( $L_s = 75^\circ\text{--}95^\circ$ ) during the reappearance of the DHL. The image N1884018021\_1 is one of the very last observations of Titan before the end of the Cassini mission in 2017 September.

### 3.4. Period 4: Reappearance of a New and Weaker Detached Haze Layer Around the Summer Solstice (2015–2017)— $L_s = 75^\circ\text{--}95^\circ$

The first occurrence of the stable detached haze in this period was seen on 2015 December 3rd (Figure 8(a)). It does not at first appear different from the previous sporadic detached haze layers observed in the period 2012–2015. Its signature is very weak, but, after this observation, the detached haze was more pronounced, and was present in each subsequent observation. The detached haze became stable over time, similarly to the detached haze before the equinox. Therefore, we consider this date as a limit to the beginning of the reappearance of the detached haze ( $L_s = 74^\circ$ ). The evolution of the haze during this period is displayed in Figure 8. These observations validate the

long-awaited reappearance of the detached haze layer, just before the end of the Cassini mission in 2017 September.

The detached haze layer is not very well defined, but can be perceived at all latitudes at around 490–520 km (Figure 8(a)). We notice a contraction the main haze: the top of the haze dropped by 50 km in 2016 January, as compared to 2015 October (Figure 7(d)). The main elements of the reappearance (altitude and date) confirm the predictions made by the general circulation models (Lebonnois et al. 2012; Larson et al. 2015) and the prediction reported in West et al. (2011). A detailed comparison between the observations and the GCM is discussed further in Section 5.

Over time, the detached haze layer became more distinct, and the zone of depletion more pronounced, especially in the

northern hemisphere (Figure 8(b)). The situation seems to be analogous to an early stage of the structure observed in 2004 (Figure 5(a)), but in the opposite hemisphere. However, although the detached haze persists over time, it also settles and almost merges with the main haze by 2016 October (Figure 8(c)). In subsequent observations (Figures 8(d) and (e)), we are witnessing the complex evolution of a newly-formed detached haze, merging with the main layer southward of 35°N while remaining stable around 450 km northward of 35°N, and which seems to vanish in 2017 May rather than settling. This structure was still observed in the very last image of Titan taken by Cassini just before its final plunge into Saturn (Figure 8(f)) in 2017 September.

A secondary detached haze layer appeared in 2016 October in the southern hemisphere at high altitude (around 520 km in Figure 8(c)). Its northern boundary is not well defined. This new structure was persistent over time, at planetary scale, up to the end of the Cassini mission, but gradually descended. The results reported by West et al. (2018) concern the detached haze at the equator only. Although they had already revealed the complex behavior of the detached haze layer, the present observations show a dichotomy between the two hemispheres. The details of this evolution, the split in the double layer structure, and the formation and disappearance of several structures, were completely unexpected. According to the GCMs mentioned above, six years after equinox, the post-equinoctial circulation was supposed to be already installed, with a planetary-scale circulation cell from the southern hemisphere to the north polar region. Apparently, this is not the case, based on the observations.

Cassini's observations from 2004 to 2017 do not completely cover half a Titan year. The first and last observations were taken almost at opposite seasons,  $L_s = 297^\circ$  and  $94^\circ$ , respectively (i.e.,  $157^\circ$  apart). This prevents direct comparisons of the detached haze at opposite seasonal phases, although both 2004 and 2017 images were captured more than a season after the previous solstice.

#### 4. Local and Short-term Variability of the Detached Haze Layer

So far, we have considered the evolution of the detached haze layer in the context of seasonal change. We then discussed its long term evolution at the planetary scale as a function of latitude. In this section, we consider sets of observations to characterize the short-term and local behavior of the detached haze. These characterizations could only be conducted based on a limited number of observations, and require very specific acquisition geometries. These allow us to observe localized, secondary order variations of the detached haze layer. Firstly, we choose several images taken a few hours apart to evaluate the hourly variability of the detached haze. Next, we consider observations at low phase angle, which simultaneously show the two limbs of Titan. And, finally, we consider observations taken from a near-polar point of view, which can show longitudinal variations in a narrow range of latitudes.

##### 4.1. Short Time or Spatial Variability

As presented above, we observed the large-amplitude variability of the detached haze layer extinction profile at all latitudes below 35°N (Figures 5(a)–(c)) between 2004 December and 2005 June. Fortunately, in 2005 June, Cassini

**Table 1**  
Sequence of 9 Images of Titan Taken 2005 June 4th

Image ID	Time (UTC)	Phase	Longitude (Eq)	Local Time (Eq)
N1496548825_1	03:32	10.4°	10.7°W	17:12
N1496552665_1	04:36	10.3°	10.4°W	17:17
N1496557465_1	05:56	10.1°	10.6°W	17:23
N1496562265_1	07:16	9.9°	13.1°W	17:17
N1496567065_1	08:36	9.8°	13.4°W	17:23
N1496571865_1	09:56	9.8°	13.9°W	17:23
N1496576665_1	11:16	9.8°	14.3°W	17:30
N1496581465_1	12:36	9.9°	14.7°W	17:30
N1496586265_1	13:56	10.1°	15.2°W	17:36

**Note.** The longitude and local time are given for the profile at the equator on the illuminated side of Titan.

captured a series of 9 images of Titan, with a time-step of 80 minutes (Table 1).

Using multiple observations of Titan over a short period, we are able to validate our calibration, and observe short time and local variability. Here, we analyze the sequence at three different locations on the limb ( $40^\circ\text{S}$ ,  $0^\circ$ ,  $40^\circ\text{N}$ ). The 9 observations are made with phase angles of around  $10^\circ$ , within an interval of  $0.6^\circ$ . The limb longitude of the observations varies between  $10^\circ\text{W}$  and  $15^\circ\text{W}$ , whereas the solar local time on Titan varies between 17:12 and 17:36.

Figure 9 presents extinction profiles extracted from the analysis of these 9 images. Firstly, we confirm that our calibration method is reliable from one image to another, and that the overall variability of the detached haze is very small. We observe the double layering at  $40^\circ\text{S}$  and  $40^\circ\text{N}$  reported previously. All the locations of the maximum of the extinction peaks are located within a small altitude range (smaller than the 8 km of the pixel scale). The vertical offsets observed at different times are consistent with the accuracy of the image navigation, and are therefore not significant. At the equator and at  $40^\circ\text{S}$ , the detached haze layer is well detached for all the profiles. When the vertical offset is accounted for, all the extinctions are found to have relative differences of about  $\pm 10\%$  compared to the average value, except in the depletion zone between the main and detached haze layers, where difference can reach an order of magnitude (at  $0^\circ$ ) to several orders of magnitude ( $40^\circ\text{N}$ ). The variations outside the depletion zone are not significant.

The variability in the depletion zone at the equator is about one order of magnitude, and consistent with uncertainties reported in Figure 4. The variability observed at  $40^\circ\text{N}$ , in the depletion zone at around 460 km are significant for two reasons. Firstly, the differences are much larger than the expected uncertainty in this zone. Secondly, the sequence shows a gradual and consistent increase of extinction with time. If these differences were due to uncertainties in the retrieval procedure, it would rather have resulted in a chaotic evolution of the extinction over time.

Furthermore, the corresponding extinction map (Figure 5(c)) shows that in the south, the detached haze layer is well separated from the main haze layer by a well-defined depletion zone. In the north, the depletion zone is less well defined, and the detached haze and the main haze are connected vertically by a residual haze. The variation in this residual haze is as reported in Figure 9 at  $40^\circ\text{N}$ . We cannot strictly determine if

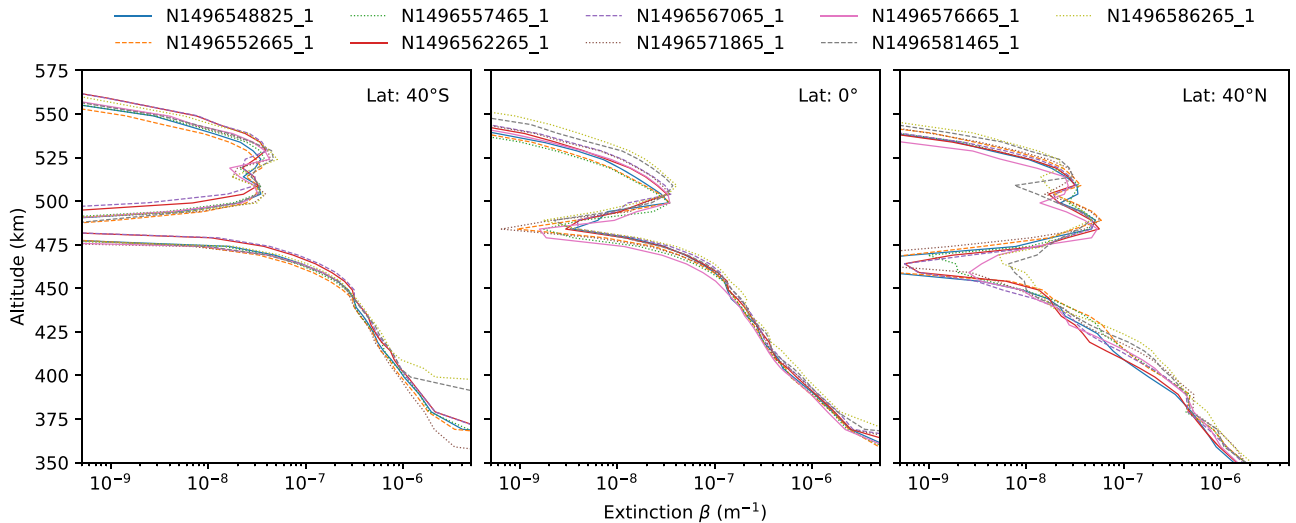


**Figure 9.** Extinction profiles for the series of 9 images taken 80 minutes apart in 2005 June (see Table 1). The global latitudinal map is shown in Figure 5(c).

we are witnessing time or spatial variations, since both the time and the longitude of the observations change simultaneously during the image sequence. We note that a rotation of  $5^\circ$  in longitude corresponds to a maximum shift of 250 km in distance (one tenth of Titan's radius), possibly consistent with a spatial variation in haze extinction.

#### 4.2. Dawn and Dusk Sides

Aside from short time and local variations, we are also interested in images showing the two sides of Titan simultaneously. At low phase angle, the viewing geometry allows us to retrieve the haze extinction with both the illuminated and the dark side of Titan simultaneously (Figure 10). In this case, we can compare the dawn and dusk limbs for specific latitudes. Although Titan's day is about 16 terrestrial days, the time spent by the haze on the night side or dayside is much shorter. Firstly, the atmosphere is superrotating, and at altitudes of around 400 or 500 km, the zonal wind is comparable to or larger than the rotation speed at ground level (Flasar et al. 2005; Achterberg et al. 2011; Lebonnois et al. 2012; Lellouch et al. 2019). This makes the actual diurnal cycle for the high altitude hazes shorter than 16 days by a factor of 2 or more. Secondly, at high altitude, sunlight penetrating beyond the geometric terminator further shortens the time spent in darkness. Thus, effects on the haze should be produced by processes with timescales comparable with a terrestrial day.

Figure 10(a) presents the haze extinction at the dawn and dusk sides, as observed in 2005 June (Figure 5(c)). The detached haze differs significantly between the two sides. At the equator, we observe on the dawn side a double detached layer of 40 km thickness, whereas it appears as a thin layer of 10 km thickness on the dusk side. The haze extinction at the peak differs significantly, from  $7 \times 10^{-8}$  to  $2.5 \times 10^{-8} \text{ m}^{-1}$ , respectively. The depletion below the haze layer is also less pronounced on the dawn side compared to the dusk side. Although this observation was made during the period of stability for the detached haze, we observed a significant asymmetry between the dawn and dusk side. This asymmetry is also observed in all the images taken at the same moment, and which were analyzed in Section 4.1.

Two years later, another low phase angle image was recorded (Figure 10(b)). This time, the detached haze layer is

much more symmetrical between the two sides. The peaks of haze extinction are at the same altitude, with comparable values. However, small differences can be noticed: there is a small secondary layer above the detached haze layer at the dusk side between  $50^\circ\text{S}$  and  $20^\circ\text{N}$ , and may even extend northward. In the northern hemisphere, the extinction appears slightly larger at dawn than at dusk, and the vertical extent of the detached haze is also a bit larger. However, the overall morphologies are very similar.

At the equinox, the detached haze layer has already started its drop in altitude (Figure 10(c)). There are significant differences between the two sides, in both hemispheres, while at the equator the two profiles are almost identical. The haze layer is not exactly symmetrical in the southern hemisphere. The detached haze itself is at the same altitude, but the depletion zone is at a higher altitude on the dawn side, and the main haze layer is thinner on the dusk side. In the northern hemisphere, the haze layer is more complex, and the asymmetry is even more marked, with a detached haze at different altitudes, and with a different extinction. The detached and main haze layers at the dawn side appear optically thicker than the layers at the dusk side. This is consistent with the two previous cases.

After the equinox, fewer images were taken at low phase angle. In these, we do not notice any significant differences between the dawn and dusk sides. After the reappearance of the detached haze layer in 2016, we found only one image with the relevant geometry to see both sides of Titan illuminated at the same time (Figure 10(d)). In this case, we are close to the solstice, and the sub-solar latitude is almost at its maximal extent and does not allow us to probe the southern high latitudes near the terminator. The main haze appears very symmetrical on both sides, and almost identical above  $45^\circ\text{N}$ . The depletion can be followed continuously all around the North Pole. At latitudes lower than  $45^\circ\text{N}$ , the values of the haze extinction are similar, but the altitudes of the extinction peak differ by 25 km.

The haze extinction profile and the altitude of the detached haze layer can differ between the dawn and dusk sides. In general, we notice a higher extinction in the dawn side than on the dusk side. This effect could be due to a diurnal cycle.

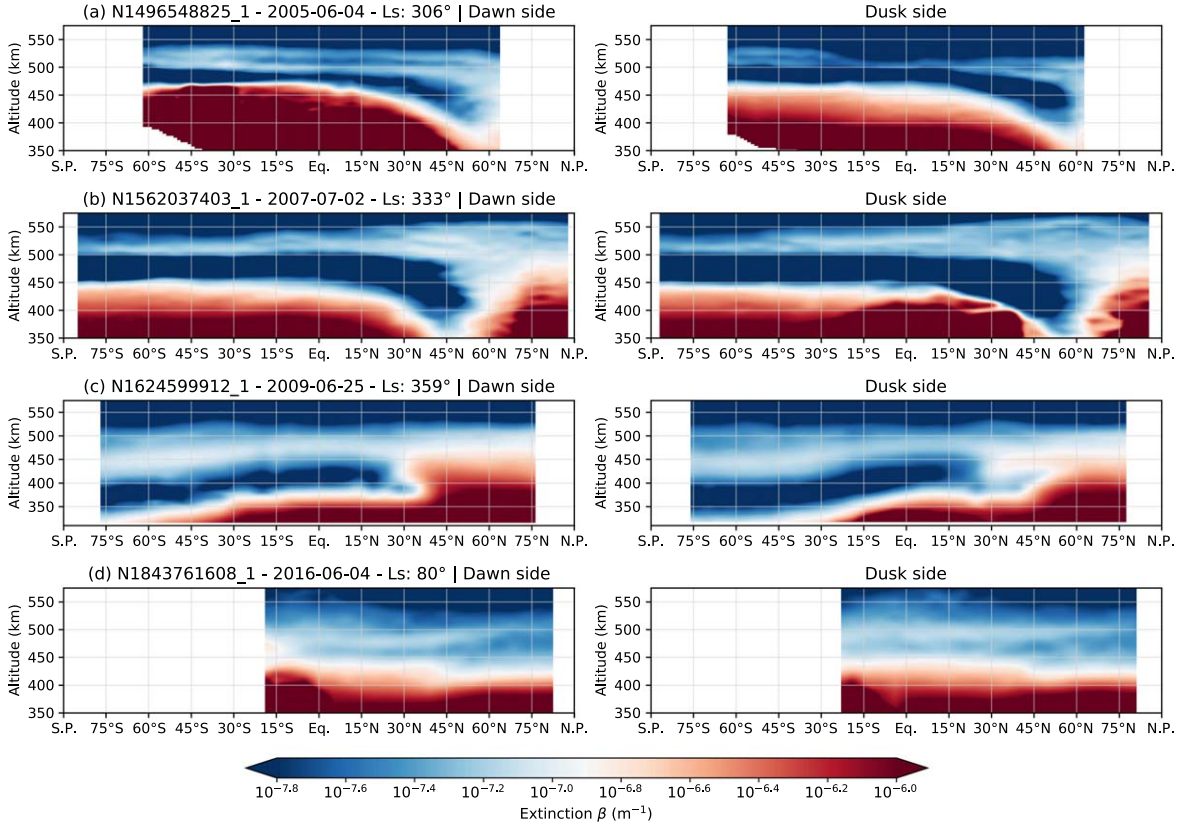


**Figure 10.** The left and right panels show maps of the haze extinction for the dawn and dusk side of Titan for 4 different images taken during the mission, where the viewing geometry allows us to observe both dawn and dusk limbs. The date and the seasonal solar longitude are provided for each image.

#### 4.3. Longitudinal Variability

Due to orbital constraints, most of our observations sampled only a small range of longitudes. However, a few observations of Titan taken from a near-polar point of view offer a unique way to study the evolution of the detached haze with a large coverage in longitude and within a small range of latitudes. This allows us first to check the homogeneity of the haze in longitude, and also allows us to extend our previous observations between the dawn/dusk sides, with a local time coverage between 6:00 and 18:00.

We analyzed a set of three images taken sequentially within a month-long interval. The first observation was performed on the 2009 March 29th (Figure 11(a)) during the collapse of the detached haze layer. Two other observations were made, at two weeks and at one month later, with the same geometry (Figures 11(b), (c)). The detached haze layer is located at 470 km for all longitudes. Inside the depletion region, we notice a plume of haze between 400 and 440 km, and between 150°W and 220°W. In mid-April, the plume is located between 160°W and 240°W, and between 375 and 425 km. It appears disconnected and settling from the detached layer, which remains at 470 km. At the end of April, we see the extension around 410 km; it has spread between 180°W and 250°W. This aerosol plume is almost connected with the main haze.

This feature is not correlated with the local time, but remains at about the same longitude, and drifts slowly toward the West. This would correspond to a retrograde motion of about  $0.6 \text{ m s}^{-1}$ . Another solution would be prograde motion of  $6.6 \text{ m s}^{-1}$ , in phase with the sampling of 15 terrestrial days. The vertical speed, assuming that the aerosol cloud dropped from

400 to 375 km in one month, would be  $10^{-3} \text{ m s}^{-1}$ . We also identified a modulation in the extinction and in the geometrical thickness of both the detached haze layer and the main haze. In the last image, only the geometrical thickness is modulated and not the haze extinction.

These observations show that the haze layer is not completely homogeneous in longitude and has some fluctuations in extinction and in geometry. It also strengthens the idea that space and time variations, as in previously discussed observations, cannot be distinguished without additional observations (not available in this data set). The dawn/dusk differences and the short-term variations, presented in the two previous subsections, could be due to longitudinal effects rather than to time variations. Therefore, with regard to the results in this section, we stress that the longitudinal inhomogeneities should be kept in mind as a secondary effect when discussing and comparing latitudinal maps of the detached haze layer.

#### 5. Comparisons with UVIS Occultations and GCM Predictions

West et al. (2018) have already confirmed the excellent agreement between the observations made during the two Voyager flybys, and the position of the detached haze layer one Titan year later. Comparisons with Cassini's Visual and Infrared Mapping Spectrometer and Cassini's Composite Infrared Spectrometer instruments may be possible, but are limited by the sensitivity of their detectors above 450 km, where the detached haze is located. Therefore, we only performed a comparison with two stellar occultations made by the Cassini Ultraviolet Imaging Spectrograph (UVIS)

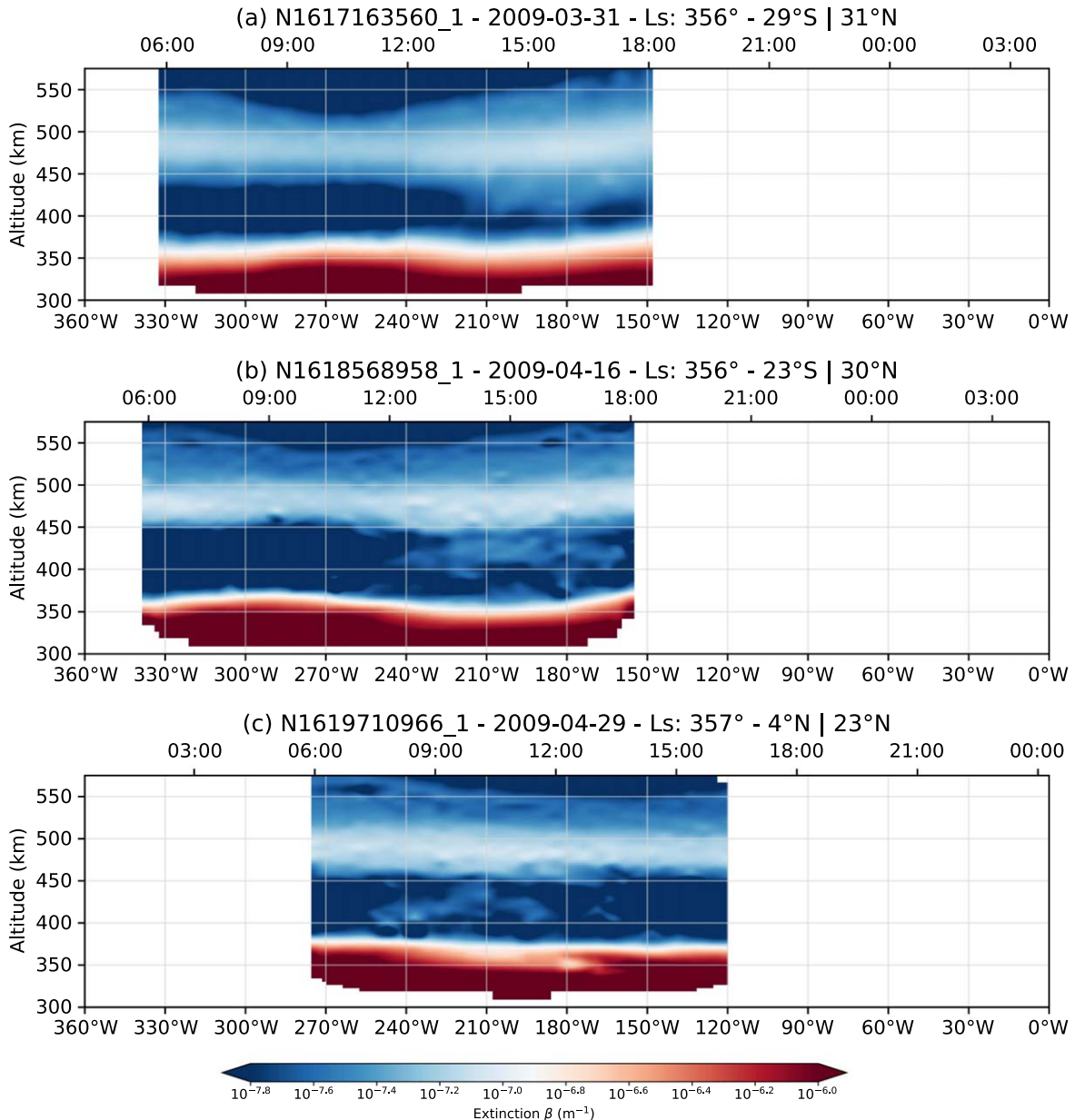


**Figure 11.** Map of the haze extinction as a function of longitude and local time for a set of 3 images taken in 2009 March and April ( $L_s = 356^\circ$ ). The latitude range covered is also indicated for each image.

instrument in 2009 (Koskinen et al. 2011). The extinction profiles retrieved in the previous sections can also be compared with results obtained with other instruments and with Global Circulation Model (GCM) predictions.

### 5.1. Comparison with UVIS Occultations

Koskinen et al. (2011) derived information on the mesosphere and thermosphere of Titan using UVIS stellar occultations. The sensitivity to haze opacity of the UVIS during a stellar occultation is much better than what the ISS can achieve. However, while the ISS probes the light scattered by the detached haze layer, the UVIS probes the light transmitted through a tangential path at the limb. In both cases, an extinction profile can be retrieved. The ISS can retrieve the extinction of those particles which scatter light, and under certain assumptions concerning phase function and single

scattering albedo (Seignovert et al. 2017; West et al. 2018). On the other hand, the UVIS is able to retrieve the total extinction from transmission, with no assumptions about the haze particles. This difference is valuable because it may provide information about changes in aerosol size with altitude. In practice, ISS sensitivity is not sufficient to probe above the peak of the detached haze by more than a scale height.

Two of the UVIS occultation profiles, in 2008 and 2009 (T41 and T53 flybys), can be directly compared with ISS observations at the same location and at the same period (Figure 12). The UVIS profiles are scaled to offset the spectral dependence between ISS and UVIS effective wavelengths (338 nm and 1850–1900 Å, respectively). This offset is due to the spectral dependence of the extinction cross-sections and to the intrinsic differences arising from comparing the extinction retrieved from scattering properties or from occultation (see Cours et al. 2011).

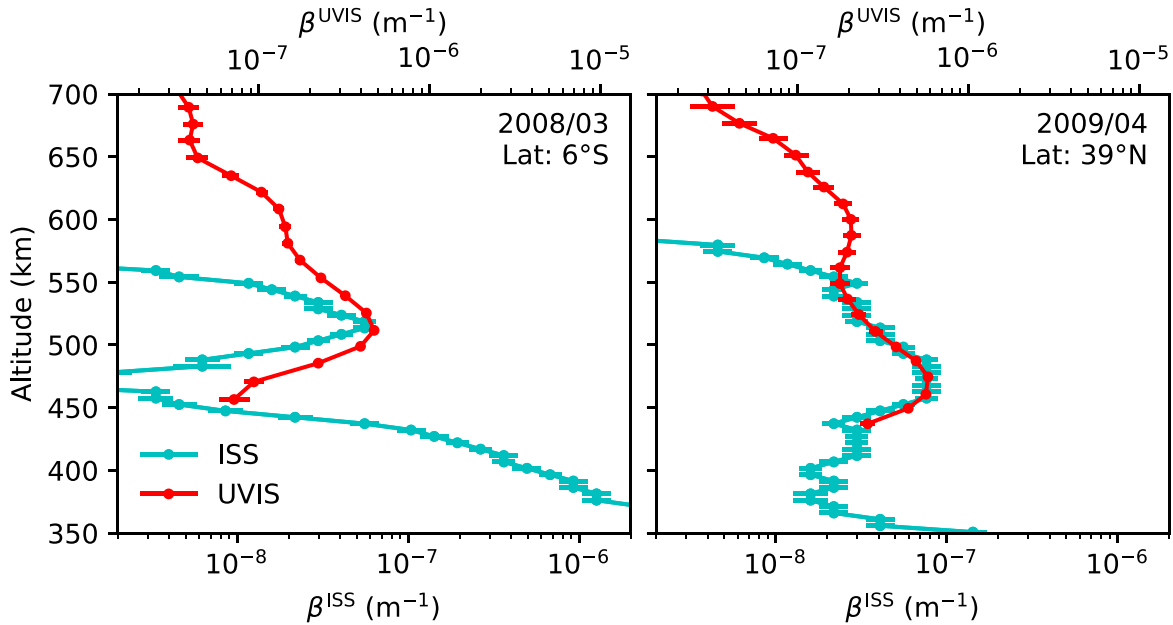


**Figure 12.** Comparisons between ISS and UVIS extinction profiles before the equinox. UVIS profiles are retrieved by Koskinen et al. (2011) during the T41 (2008 February 23) and T53 (2009 April 19) flybys. ISS profiles are retrieved for the images N1585329510\_1 (2008 March 27) and N1618568958\_1 (2009 April 16). The UVIS profiles are scaled by a factor of 0.15 to compensate for the spectral dependence of the extinction cross-section and overlap ISS retrievals.

The two profiles can be compared in the 450–550 km altitude range. In the first case (Figure 12(a)), even if the profiles do not exactly overlap, the ISS extinction profile presents a peak of extinction exactly at the same location as that observed via UVIS. The drop, both above and below the peak, is more pronounced with ISS than with UVIS. In the second case (Figure 12(b)), the two profiles present an excellent agreement with one another in the 450–550 km altitude range.

Considering that the UVIS and ISS profiles are not taken simultaneously, and do not probe the same longitude, the results of the previous section demonstrate that these differences are consistent with the natural variabilities observed in the detached haze layer. This comparison is then a good validation of our results concerning the extinction profiles of the detached haze.

Above 575 km, the UVIS extinction profiles show the presence of a secondary layer at 610 km which is not detected by the ISS. The ISS is sensitive to aerosols scattered throughout the limb, whereas UVIS observations probe the extinction along the tangential path. Due to its stronger forward scattering peak, the larger particles contribute more to the measured ISS scattering signal, as compared to the smaller particles, which scatter the light more isotropically. During an occultation, both small and large particles contribute to the UVIS extinction signal (Cours et al. 2011). In theory, the difference between UVIS and ISS profiles above 575 km could reveal a change in aerosol size distribution. However, this layer is located at altitudes where the signal to noise is low, and where our model is no longer able to retrieve the extinction properly. Therefore, it is not possible to draw a safe conclusion from a comparison between ISS and UVIS profiles above 575 km.

## 5.2. Comparison with General Circulation Model Predictions

General circulation models are very powerful tools to enable an understanding of the climate of planetary atmospheres and the interplay between different processes at planetary scales. In

the case of Titan, circulation and haze are linked by a strong feedback loop. The large-scale structures in the haze layer are produced by the action of circulation. The haze layer produces a feedback effect on the circulation via control of the stratospheric thermal structure (Rannou et al. 2004). The detached haze is one of the noticeable features produced by the stratospheric circulation (Rannou et al. 2002; Lebonnois et al. 2012; Larson et al. 2015). Figures 13 and 14 show the maps of haze extinction obtained by Lebonnois et al. (2012) and Larson et al. (2015) at 700 nm and 525 nm, respectively. Similarly to the comparison with UVIS, the distribution of the haze from the GCMs can be compared with the extinction map derived with ISS in the CL1-UV3 filters at 338 nm with a scaling factor.

At the northern winter solstice (Figure 13), the detached haze appears at around 350 km in both models. In Lebonnois et al. (2012), the altitude decreases by a few tens of km from the southern latitudes to the north polar region, where it merges with the north polar hood at 40°N (Figure 13(a)). In Larson et al. (2015), the detached haze remains at a constant altitude (Figure 13(b)), appears better marked than in Lebonnois et al. (2012), and merges with the polar hood at around 60°N. In both models, the extinction increases from the south to the north by about half an order of magnitude. In the ISS observations made in 2004 (Figure 13(c)), i.e., in the middle of winter, the detached haze layer is completely developed at 500 km and covers latitudes from the south polar region to 60°N, where it merges with the north polar hood. The location of the depletion zone decreases from 475 to 425 km between 40°N and 60°N, which is not the case in the models. It is, on the other hand, consistent with the results obtained from stellar occultation by Sicardy et al. (2006). The haze extinction increases from the south to the north with about the same magnitude as in the models. This is consistent with a layer increasing in aerosol loading while the airmass is flowing from south to north. As already noted (West et al. 2011, 2018), the detached haze layer in the models appears as a supplementary layer added to the

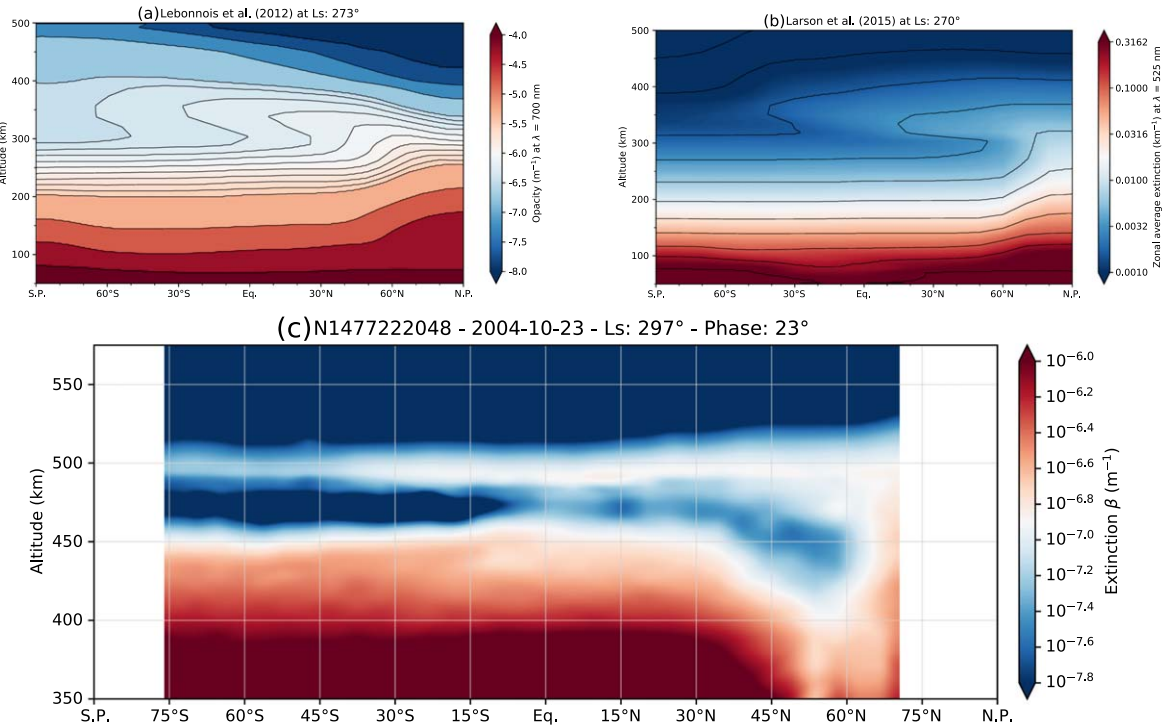


**Figure 13.** Zonally averaged haze extinction at northern winter solstice ( $L_s = 270^\circ$ ), estimated by Lebonnois et al. (2012) at the wavelength  $\lambda = 700$  nm (a), and by Larson et al. (2015) at  $\lambda = 525$  nm (b). (c) Haze extinction map retrieved from Cassini/ISS observation CL1-UV3 ( $\lambda = 338$  nm) in the middle of winter (N1477222048\_2— $L_s = 300^\circ$ ).

background aerosols, whereas in the data, it appears detached because there is a zone strongly depleted in aerosols. Finally, as mentioned above, the detached haze layer is continuous all around the South Pole, which is not the case in the models.

At the northern spring equinox (Figure 14), the model of Lebonnois et al. (2012) shows a flat main haze layer without a detached haze between  $60^\circ\text{S}$  and  $60^\circ\text{N}$ , and with two major increases at both poles (Figure 14(a)). The haze in the south is increasing as a consequence of the circulation reversal, while the northern haze is diminishing, and will disappear later in the season. In the observations (Figure 14(c)), this thicker haze is observed only for northern latitudes, the detached haze has not yet disappeared, and the feeding of the south polar haze has not started. To observe a major increase of extinction at the South Pole, we need to wait until the beginning of spring at  $L_s = 30^\circ$  (Figure 14(d)). At that time, the detached haze layer has almost completely collapsed into the main haze and the haze distribution is very similar to that predicted by Lebonnois et al. (2012) at the equinox (Figure 14(a)). In Larson et al. (2015), 1000 days after the equinox (Figure 14(b)), we also observed a *U* shape in the meridional haze extinction distribution, as in the data (Figure 14(d)), but in this case, a new detached haze layer has already started to grow from the South Pole in the model (Figure 14(b)), whereas in the data (Figure 14(d)) the local increase seen at 380 km is the consequence of a drop in a previous secondary layer (see Figures 6(g) and (h)). In both comparisons, this means that the timing in the circulation models is not completely in phase with that of the observations. The model of Lebonnois et al. (2012) seems to be in advance by about three years, as compared to the data. We do not have enough information to characterize the advance in phase of the model of Larson et al. (2015).

Anticipated in late 2014 or early 2015 ( $L_s = 60^\circ$ , Figure 15(a)) by Larson et al. (2015) or in mid-2017 ( $L_s = 90^\circ$ , Figure 15(b))

by Lebonnois et al. (2012), the detached haze layer finally reappeared in late 2015 to early 2016 ( $L_s = 74^\circ$ , Figure 15(c)). However, in 2017 May, the upper atmosphere of Titan was still evolving, and did not show a polar hood in the South Pole similar to that observed in 2004. Moreover, the most recent observations of early-2017 (Figures 8(c) and (d)) seem to show that the seasonal formation of the detached haze layer could be different from one hemisphere to the other. The double peaks at 420 and 450 km in the temperature gradient profile, a proxy for the haze extinction, obtained from the 1989 occultation (Sicardy et al. 1999) supports this hypothesis.

The current general circulation models do not match some of the large-scale features reported earlier. The first of these is the shape of the vertical extinction profile, which has a local depletion, producing the appearance of a detached haze layer in the observations, while in the models it appears as a high altitude haze layer, superimposed onto the main background haze. The amplitude of the observed depletion, reported before and during the collapse, is sufficient to consider that the detached haze layer is really disconnected from the main haze layer. We have already stressed that the detached haze layer is continuous around the South Pole, without any visible upwelling coming from the main haze at this location. Finally, we reported an early contraction of the main haze in 2008, just before the drop in the detached haze at the equinox. The origin for such a contraction is likely to be related to the weakening of the Hadley cell when the latitudinal illumination gradient decreases around the equinox.

Thanks to high spatial resolution of the ISS/NAC camera, we noticed some small-scale structures which could be unresolved or erased by the temporal averaging in GCMs. During the northern winter and spring, we observed some sporadic decreases and bursts in the extinction profiles at very short timescales. These events could have a major impact on

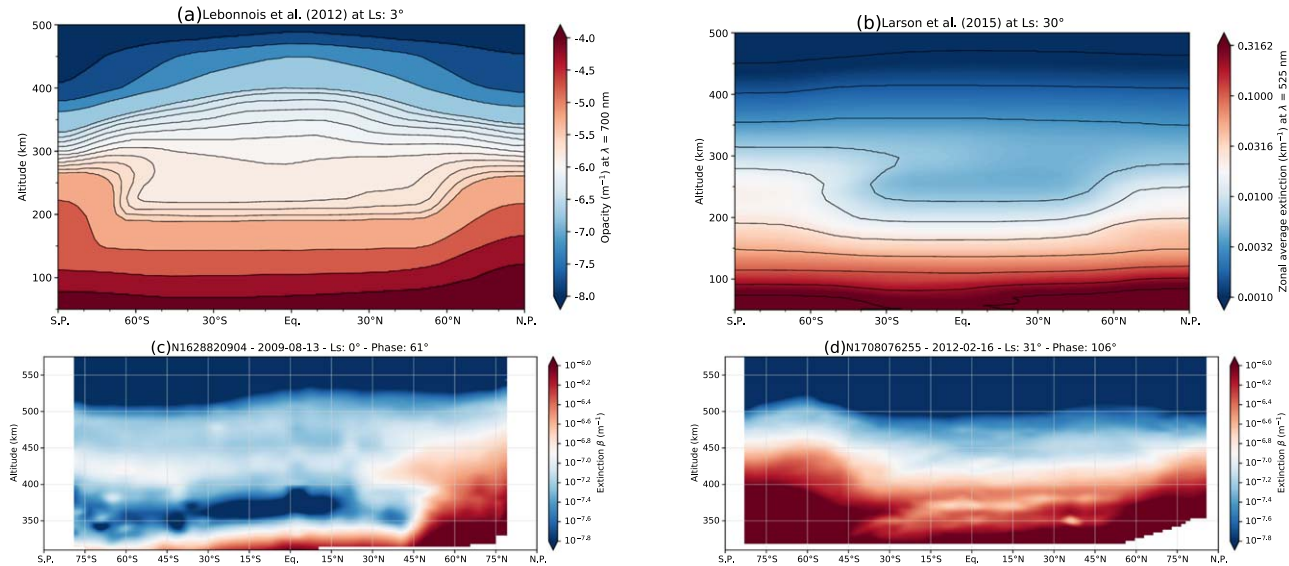


**Figure 14.** Rescaled zonally averaged haze extinction at the northern spring equinox ( $L_s = 3^\circ$ ), estimated by Lebonnois et al. (2012) (a), and at 1000 days after the equinox ( $L_s = 30^\circ$ ) by Larson et al. (2015) (b). (c)–(d) Haze extinction map retrieved from the Cassini/ISS observations at the Northern Spring equinox (N1628820904\_1— $L_s = 0^\circ$ ) and 1000 days after the equinox (N1708076255\_1— $L_s = 30^\circ$ ).

the redistribution of aerosols in the upper atmosphere. We also reported, for numerous cases, the existence of sub-layers above the main detached haze layer, with large latitudinal extension. Usually, their presence could be followed for more than one Earth year. This is especially true during the collapse of the main detached haze layer after the equinox, where we observed several smaller drops from 500 km down to 300 km. Finally, the double structure reported in early-2017 (Figures 8(c) and (d)) with two very distinct detached haze layers in the North at 450 km, in the South at 520 km, has never been mentioned before, and is not reported in the current GCMs. New modeling with a better vertical resolution will be required to interpret this structure.

We want to highlight facts that would help to better constrain the climate models. GCMs are ideal tools with which to understand the interplay of different components of Titan's climate. However, they also have several limitations which are often technical in nature (low spatial resolution, shallow water approximation for the dynamics, radiative transfer in plane-parallel, no link with the high mesosphere and thermosphere physics). Limitations may also come from incorrect boundary conditions. We make the following remarks:

1. the collapse starts in the southern hemisphere, and concerns the main haze, followed by the detached haze. This may indicate that aerosols of the main haze and the detached haze do not have the same fractal structure. This has previously been suggested by Lavvas et al. (2009) and Larson et al. (2015). The weakening or the displacement of the ascending branch of the circulation would first affect the more compact aerosols of the main haze, prior to the fluffiest aerosols of the detached haze, which can more easily remain suspended.
2. the finest details found in this work occur at length scales smaller than the GCM grid scale. ISS observations show an instantaneous snapshot of the haze layer. GCMs generally calculate extinction of haze averaged over several Titan days and/or are zonally averaged. Comparing the GCMs' instantaneous and not zonally averaged outputs would allow us to see whether or not they are

able to produce the same kind of variabilities as observed. These variabilities may also be induced by processes occurring in higher layers not modeled by the GCMs.

3. the timing offset of the DHL reappearance in the GCM is probably due to the model's top levels, which are generally too low. Vertical extension of the models and of the haze layer may improve the timing of the cycle.
4. the source of the aerosols depends on photochemical processes that occur far above the DHL, and which are also subjected to circulation in the upper mesosphere and thermosphere. Accounting for the physics and chemistry in higher layers, for instance, a coupling with thermospheric models could be key to a further understanding of the details of the haze cycle.

## 6. Conclusions

In this article we have analyzed observations of light scattered at the limb of Titan with ISS (UV3 filter) on the Cassini spacecraft. We retrieved the haze extinction as a function of altitude, latitude, and time between 2004 October and 2017 September. We followed, during the course of about half of Titan's year, the evolution of the DHL and the top of the main haze. In particular, we witnessed the collapse of the DHL during the equinoctial transition of the atmospheric circulation, and its reappearance before the following solstice.

We confirmed and provided details about the collapse of the detached haze layer, previously reported by West et al. (2011). We also tracked the small-scale variations after the equinox in order to detect the reappearance of the detached haze layer at the end of 2015 (West et al. 2018). These two previous works focused on the DHL at the equator. Here, we give a full description of the structures of the haze layer as a function of altitude, latitude, and time. We find that the DHL has a natural variability, which can be both temporal and spatial, and sometimes two distinct hazes or plumes can be observed above the DHL. The amount of data is not large enough to distinguish between spatial or longitudinal variability. However, data taken

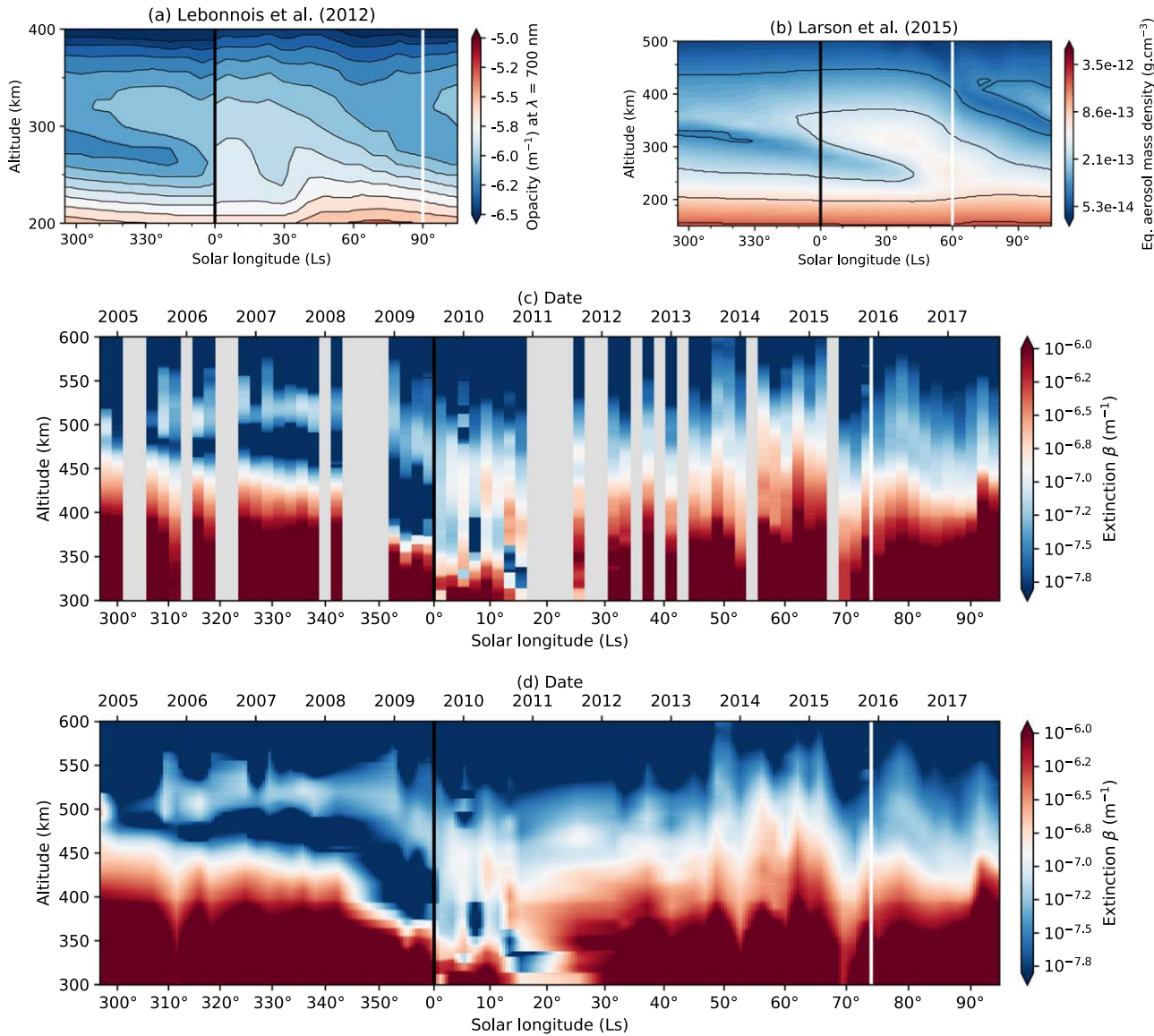


**Figure 15.** (a) Annual variations of the zonally averaged equatorial opacity at 700 nm, extracted from Lebonnois et al. (2012) and wrapped around  $L_s = 0^\circ$ . (b) Seasonal evolution of the aerosol mass density ( $\text{g cm}^{-3}$ ) adapted from Larson et al. (2015). (c) The haze extinction coefficient as a function of time and altitude at the equator (this work). The data are binned by 2 months ( $\Delta L_s \approx 2^\circ$ ). The gray area corresponds to the period where no UV3 observations were available (see Figure 3). (d) Same results as middle panel, but linearly extrapolated in the area without observations. This plot is only provided as an indicative global pattern, but contains obvious interpolation artifact. In each panel, the black vertical line corresponds to the vernal equinox ( $L_s = 0^\circ$ ), and the white vertical line is the date of the reappearance of the detached haze layer ( $L_s = 90^\circ$ ,  $L_s = 60^\circ$ , and  $L_s = 74^\circ$ , respectively).

from a polar viewpoint indicates that the haze is not completely uniform in longitude.

The equinoctial collapse starts in the summer hemisphere. Its initial phase can be discerned from 2008 March. The main haze collapses first, and the detached haze layer about one terrestrial year later. By 2012 April, the detached haze is below 300 km and cannot be seen at UV wavelengths. The fall of the detached haze layer between 2009 and 2011 occurred at an average speed of  $-67 \text{ km yr}^{-1}$ . During the equinoctial collapse, the DHL seems to settle down at the aerosol terminal speed, as reported by West et al. (2018). If sedimentation does control the speed of the collapse, this would indicate an absence of vertical wind at these two moments. During a period of three and a half years (from mid-2011 to 2015), no stable detached haze layer was observed. However, the haze layer fluctuates, and sporadic local detached layers appeared and disappeared rapidly.

The detached haze layer reappeared in 2015 December. We first noticed this new detached haze when it was marginally apparent in UV3 images. The timing of the reappearance is offset compared to GCM predictions, and occurs with patterns more complex than those predicted. It first reappeared at around 500 km in 2015 December ( $L_s = 74^\circ$ ) as a very faint structure, which became persistent and more pronounced with time. At the equator this structure sedimented, and finally disappeared in about one year, whereas it remained visible in the northern hemisphere. A second detached haze appeared in 2016 July at around 500 km altitude, above the first DHL, and apparently started to settle down as well. Unfortunately, the survey was interrupted in 2017 September by the end of the Cassini mission. This second detached haze layer did not cover all latitudes, was quite variable, and was present up to the final observation.

Unfortunately, no data were acquired between 2008 April and 2009 February, or between 2010 December and 2011

September. We thought to use the NAC UV1 and UV2 images, but these data have a very poor signal to noise ratio and cannot be included in our analysis. However, a few images are available from the WAC camera in the VIO (Violet), BL1 (Blue) filters. The behavior of the aerosols at these wavelengths should be very similar to those of the UV3 filter, and could fill these gaps. It would also be interesting to perform a similar analysis with data acquired through filters at larger wavelengths. In this case, it would be possible to probe deeper layers in order to monitor the collapse of the DHL further down and, in addition, the cycle of the main haze. For instance, Rages & Pollack (1983) could probe as low as 200–250 km with a clear filter ( $\lambda_{\text{eff}} \simeq 0.5 \mu\text{m}$ ). At even longer wavelengths, we could reach levels in the low stratosphere, and maybe probe high altitude polar clouds (de Kok et al. 2014; West et al. 2016).

Comparisons with General Circulation Models are fruitful. Our results reinforce the scenario of a detached haze cycle primarily controlled by circulation, as proposed by Toon et al. (1992) with a 1D model, Rannou et al. (2002) with a coupled 2D-GCM, and Lebonnois et al. (2012) and Larson et al. (2015) with coupled 3D-GCMs. Although GCMs capture the global haze cycle, many differences remain, mainly driven by technical limitations.

This work was supported by the French Ministry of Public Research. The authors also thank the Programme National de Planétologie (PNP) for their financial support. B.S. and R.W. thank the Cassini Mission, particularly in regard to the advocacy of Trina Ray and Mou Roy, for obtaining the images studied here. Part of this work was performed by the Jet Propulsion Laboratory, California Institute of Technology, under a contract with the National Aeronautics and Space Administration (80NM0018D0004). P.R. and S.V. thank the French Agence Nationale de la Recherche (ANR Project APOSTIC No. 11BS56002, France). B.S. thanks the Planetary Rings Node (SETI Institute) for their excellent PDS browser interface, OPUS.<sup>5</sup>

## Data Availability

A list of all ISS images and UV extinction profiles derived from this analysis, plus the source code to produce the figures, will be made publicly available after publication on the Caltech Data Archive,<sup>6</sup> doi:10.22002/d1.1344.

<sup>5</sup> <https://tools.pds-rings.seti.org/opus>

<sup>6</sup> <https://data.caltech.edu>

## ORCID iDs

- Benoît Seignovert <https://orcid.org/0000-0001-6533-275X>  
 Pascal Rannou <https://orcid.org/0000-0003-0836-723X>  
 Robert A. West <https://orcid.org/0000-0002-4320-2599>  
 Sandrine Vinatier <https://orcid.org/0000-0001-5541-2502>

## References

- Achterberg, R. K., Giersch, P. J., Conrath, B. J., Michael Flasar, F., & Nixon, C. A. 2011, *Icar*, **211**, 686  
 Acton, C. H. 1996, *P&SS*, **44**, 65  
 Annex, A., Pearson, B., Seignovert, B., et al. 2020, *JOSS*, **5**, 2050  
 Bézard, B., Vinatier, S., & Achterberg, R. K. 2018, *Icar*, **302**, 437  
 Chassefière, E., & Cabane, M. 1995, *P&SS*, **43**, 91  
 Cours, T., Burgalat, J., Rannou, P., et al. 2011, *ApJL*, **741**, L32  
 de Kok, R. J., Teanby, N. A., Maltagliati, L., Irwin, P. G. J., & Vinatier, S. 2014, *Natur*, **514**, 65  
 Evans, K. F. 1998, *JAtS*, **55**, 429  
 Flasar, M., Achterberg, R. K., Conrath, B. J., et al. 2005, *Sci*, **308**, 975  
 Hunt, B., Sheppard, D., & Nadar, M. 1996, in Proc. 3rd IEEE Int. Conf. on Image Processing, 3: Multiframe Poisson Map Deconvolution of Astronomical Images (Piscataway, NJ: IEEE), **109**  
 Knowles, B., West, R., Helfenstein, P., et al. 2020, *P&SS*, **185**, 104898  
 Koskinen, T. T., Yelle, R. V., Snowden, D. S., et al. 2011, *Icar*, **216**, 507  
 Larson, E. J., Toon, O. B., West, R. A., & Friedson, A. J. 2015, *Icar*, **254**, 122  
 Lavvas, P., Yelle, R. V., & Vuitton, V. 2009, *Icar*, **201**, 626  
 Lebonnois, S., Burgalat, J., Rannou, P., & Charnay, B. 2012, *Icar*, **218**, 707  
 Lellouch, E., Gurwell, M. A., Moreno, R., et al. 2019, *NatAs*, **3**, 614  
 Porco, C. C., Baker, E., Barbara, J., et al. 2005, *Natur*, **434**, 159  
 Rages, K., & Pollack, J. 1983, *Icar*, **55**, 50  
 Rages, K., Pollack, J. B., & Smith, P. H. 1983, *JGRA*, **88**, 8721  
 Rannou, P., Cabane, M., Botet, R., & Chassefière, E. 1997, *JGRE*, **102**, 10997  
 Rannou, P., Ferrari, C., Rages, K., Roos-Serote, M., & Cabane, M. 2000, *Icar*, **147**, 267  
 Rannou, P., Hourdin, F., & McKay, C. P. 2002, *Natur*, **418**, 853  
 Rannou, P., Hourdin, F., McKay, C. P., & Luz, D. 2004, *Icar*, **170**, 443  
 Seignovert, B., Rannou, P., Lavvas, P., Cours, T., & West, R. A. 2017, *Icar*, **292**, 13  
 Sicardy, B., Colas, F., Widemann, T., et al. 2006, *JGRE*, **111**, E11S91  
 Sicardy, B., Ferri, F., Roques, F., et al. 1999, *Icar*, **142**, 357  
 Smith, B. A., Soderblom, L. A., Batson, R., et al. 1982, *Sci*, **215**, 504  
 Smith, B. A., Soderblom, L. A., Beebe, R., et al. 1981, *Sci*, **212**, 163  
 Smith, P. H. 1980, *JGR*, **85**, 5943  
 Sromovsky, L. A., Suomi, V. E., Pollack, J. B., et al. 1981, *Natur*, **292**, 698  
 Toon, O. B., McKay, C. P., Griffith, C. A., & Turco, R. P. 1992, *Icar*, **95**, 24  
 West, R., Del Genio, A., Barbara, J., et al. 2016, *Icar*, **270**, 399  
 West, R. A., Balloch, J., Dumont, P., et al. 2011, *GeoRL*, **38**, 38  
 West, R. A., Knowles, B., Birath, E., et al. 2010, *P&SS*, **58**, 1475  
 West, R. A., Seignovert, B., Rannou, P., et al. 2018, *NatAs*, **2**, 495